JAERI-M
83-189

STRESS INTENSITY FACTOR ANALYSES OF SURFACE CRACKS IN THREE-DIMENSIONAL STRUCTURES

November 1983

Noriyuki MIYAZAKI,* Katsuyuki SHIBATA
Takayuki WATANABE** and Kazunori TAGATA**

日本原子力研究所
Japan Atomic Energy Research Institute

JAERI-M レポートは，日本原子力研究所が不定期に公刊している研究報告書です。
入手の問合わせは，日本原子力研究所技術情報部情報資料課（〒319－11 茨城県那珂郡東海村）あて，お申しこしください。なお，このほかに財団法人原子力弘済会資料センター（〒319-11 茨城県那珂郡東海村日本原子力研究所内）で複写による実費領布をおこなっております。

JAERI-M reports are issued irregularly.
Inquiries about availability of the reports should be addressed to Information Section, Division of Technical Information, Japan Atomic Energy Research Institute, Tokai-mura, Naka-gun, Ibaraki-ken 319-11, Japan.

編集兼発行　日本原子力研究所
印　　刷　山田軽印刷所

JAERI-M 83-189

Stress Intensity Factor Analyses of Surface Cracks in Three-Dimensional Structures

Noriyuki MIYAZAKI*, Katsuyuki SHIBATA
Takayuki WATANABE** and Kazunori TAGATA**

Department of Nuclear Safety Research,
Tokai Research Establishment, JAERI

(Received October 18, 1983)

The stress intensity factor analyses of surface cracks in various three-dimensional structures were performed using the finite element computer program EPAS-J1. The results obtained by EPAS-J1 were compared with other finite element solutions or results obtained by the simplified estimation methods. Among the simplified estimation methods, the equations proposed by Newman and Raju give the distributions of the stress intensity factor along a crack front, which were compared with the result obtained by EPAS-J1. It was confirmed by comparing the results that EPAS-J1 gives reasonable stress intensity factors of surface cracks in three-dimensional structures.

Keywords : Stress Intensity Factor, Three-Dimensional Structure, Finite Element Computer Program, EPAS-J1, Simplified Estimation Method, Surface Crack, Comparative Evaluations

---

This work was performed under the contract between the Science and Technology Agency of Japan and JAERI to demonstrate the integrity for fatigue life of the primary coolant pipes in nuclear power plants

* Department of Chemical Engineering, Faculty of Engineering, Kyushu University

** Century Research Center Corporation

三次元構造物中の表面き裂の応力拡大係数解析

日本原子力研究所東海研究所安全工学部
宮崎　則幸*・柴田　勝之・渡辺隆之**・田形　一則**

（1983年10月18日受理）

有限要素法計算プログラムEPAS－J1を用いて，三次元構造物中の表面き裂の応力拡大係数解析を行った。EPAS－J1により求められた結果を，他の有限要素解あるいは簡易解析法による結果と比較した。簡易解析法のうち，NewmanとRajuによって提案された式を用いる方法では，き裂縁に沿った応力拡大係数の分布が求められるので，この分布についてEPAS－J1による結果と比較した。これらの比較の結果，EPAS－J1は三次元構造物中の表面き裂について，ほぼ妥当な結果を与えることがわかった。

この報告書は，電源開発促進対策特別会計法に基づき，日本原子力研究所が科学技術庁からの受託研究として実施している昭和56年度配管信頼性実証試験のうち，EPAS－J1による，三次元構造物中の表面き裂の応力拡大係数解析結果をまとめたものである。

＊　九州大学工学部化学機械工学科

＊＊ センチュリリサーチセンタ㈱

CONTENTS

目　　次

List of Tables and Figures

1. Introduction

Fatigue crack growth often has ill effects on the integrity of structures, when the structures containing initially small cracks are subjected to a cyclic load condition. The Paris-Erdogen equation is exclusively used to predict the rate of fatigue crack growth. According to the equation, the crack growth per one load cycle is related to the range of stress intensity factor by an exponential function. Therefore, in the analysis of fatigue crack growth, a stress intensity factor is required for a crack shape which changes continuously because of crack growth. The stress intensity factors of various types of cracks in two-dimensional structures are given in the Tada et al.'s handbook.[1] On the other hand, very few results are available for the stress intensity factors of surface crack in three-dimensional structures except for plate.

Extensive stress intensity factor analyses were performed for various shapes of semi-elliptical surface cracks in plates and several results are expressed by the equations which are easily applicable to the analyses of fatigue crack growth. The results of semi-elliptical cracks in plates can be used to calculate the stress intensity factors of semi-elliptical cracks in other structures[2] by applying the procedure presented in ASME Boiler and Pressure Vessel Code, Sec. XI. The results obtained by the simplified estimation methods should be compared with the finite element solutions to check their accuracies.

This report presents the comparision of the stress intensity factors of surface cracks in various three-dimensional structures obtained by the simplified estimation methods and by the finite element method.

2. Stress Intensity Factor Analysis by the Finite Element Method

The finite element computer program EPAS-J1 was used to obtain the stress intensity factors of surface cracks in three-dimensional structures. The details of the program are well documented by the authors.[3] Therefore, only the outline of the program is presented here.

The EPAS-J1 program has several connection elements to connect the beam element and the three-dimensional solid element with thin or thick shell element. The Lagrange multiplier technique is employed in the connection elements to ensure the continuity of displacements between two different kinds of elements. In a surface crack problem, the three-dimensional solid elements are employed only in the neighborhood of a surface crack, while the remainder of the structure is modeled by the shell or beam elements because of the reason that the three-dimensional stress field due to a surface crack is localized near a crack front. In the stress intensity factor analyses presented in this report, the structures including surface cracks were modeled using different kinds of elements. The 16-node solid elements were used in the solid region near a surface crack. The distorted elements[4] were allocated along a crack front to take account of the stress singularity around a crack tip. In the EPAS-J1 program, the virtual crack extension method[5] was employed to calculate the stress intensity factor. This method can be easily incorporated into an existing finite element computer program and provides relatively accurate results even under coarse finite element mesh.

3. Simplified Estimation Methods for Calculating Stress Intensity Factor of Surface Crack

In order to perform two-dimensional analysis of fatigue crack growth for a semi-elliptical surface crack in a plate as shown in Fig. 3.1, the stress intensity factors should be calculated for the deepest point A and the surface point B. The stress intensity factors at the points A and B are expressed as follows, if the stress varies linearly through plate thickness.

$$\begin{cases} K_I^A = (M_m^A \sigma_m + M_b^A \sigma_b) \dfrac{\sqrt{\pi a}}{E(k)} & (3.1) \\ K_I^B = (M_m^B \sigma_m + M_b^B \sigma_b) \dfrac{\sqrt{\pi a}}{E(k)} & (3.2) \end{cases}$$

in which the superscripts A and B denote the values pertinent to the points A and B, and the subscripts m and b represent the membrane and bending components, respectively. K_I, M and σ denote the stress intensity factor, stress correction factor and stress, respectively. E(k) is the elliptic integral of second kind and can be written as

$$E(k) = \int_0^{\frac{\pi}{2}} \sqrt{1 - k^2 \sin^2 \phi}\, d\phi, \qquad k^2 = 1 - \left(\frac{a}{c}\right)^2 \qquad (3.3)$$

ASME Boiler and Pressure Vessel Code, Sec. XI, provides a procedure for calculating the stress intensity factor of a surface crack in a general three-dimensional structure. In this procedure, the actual nonlinear stress distribution should be conservatively approximated using the linearization technique illustrated in Fig. 3.2. The linearized stress distribution should then be characterized by the membrane stress σ_m and the bending stress σ_b as shown in Fig. 3.2. The stress intensity factor can be calculated by substituting the stresses σ_m and σ_b obtained by the above procedure into eqs. (3.1) and (3.2) together with use of appropriate stress correction factors.

The analytical method[6][7], the semi-analytical method or alternative method[8][9], the finite element method[10][11] and the boundary integral method[12] have been applied to the stress intensity factor analyses of a semi-elliptical surface crack in a plate. Using these results, the stress correction factors M_m^A, M_m^B, M_b^A and M_b^B are given in the form of graphs or equations as a function of a/t, a/c, etc.. In order to perform the analysis of fatigue crack growth where a crack shape

changes continuously with a load cycle, it is convienient to use the stress correction factors expressed in the form of equations. Therefore, the following six types of the stress correction factors were employed in the simplified estimation methods for calculating the stress intensity factor of a semi-elliptical crack in a general three-dimensional structure.

(1) ASME Code, Sec. XI

The stress correction factors at the deepest point A, M_m^A and M_b^A, are given in the form of graphs as shown in Figs. 3.3 and 3.4 which are conservative evaluation of Smith's results[13]. On the other hand, the stress correction factor at the surface point B, M_b^B, is given only in the case of $a/\ell=0.3$ and 0.2

(2) Sakakibara et al.'s equations[14]

Sakakibara et al. gave the following equations, mainly based on the graphs of ASME Boiler and Pressure Vessel Code, Sec. XI.

$$M_m^A = \frac{1}{\sqrt{\pi}}\left[1.95 + \left(1-\frac{a}{c}\right)^{3.5}\left\{0.04 - 0.41\left(\frac{a}{t}\right) + 18.70\left(\frac{a}{t}\right)^2 - 38.48\left(\frac{a}{t}\right)^3 + 53.85\left(\frac{a}{t}\right)^4\right\}\right] \tag{3.4}$$

$$M_b^A = \frac{1}{\sqrt{\pi}}\left[1.79 + 0.2\left(1-\frac{a}{c}\right) - 2.47\left(\frac{a}{t}\right) + \left(1-\frac{a}{c}\right)^{3.5}\left\{12.97\left(\frac{a}{t}\right)^2 - 23.17\left(\frac{a}{t}\right)^3 + 24.80\left(\frac{a}{t}\right)^4\right\}\right] \tag{3.5}$$

$$M_m^B = 1.32\left(\frac{a}{c}\right) \tag{3.6}$$

$$M_b^B = 0.8 \tag{3.7}$$

$$(0 \leq a/t \leq 0.6)$$

They also gave the following correction factor to consider the effect of the exsistence of a surface crack in a curved plate

$$f(\lambda) = 1 + \left\{0.41\,\lambda - 0.386\left(1 - e^{-1.25\lambda}\right)\right\} a/t \tag{3.8}$$

$$\lambda = \sqrt[4]{12\left(1-\nu^2\right)}\; c/\sqrt{r\,t} \tag{3.9}$$

For a surface crack in a curved plate, the stress intensity factor obtained by eqs. (3.1) and (3.2) should be multiplied by the value $f(\lambda)$. They performed the analysis of fatigue crack growth for a surface crack in an elbow using above equations.

(3) Soya et al.'s equations[15]

Soya et al. obtained the following equations, based on Shah and Kobayashi's results.[16]

$$M_m^A = \left\{1 + 0.12\left(1 - \frac{a}{2c}\right)^2\right\}\left[1.0 + \left\{0.127\left(\frac{a}{t}\right) - 0.079\left(\frac{a}{c}\right)\right\} - \left\{0.558\left(\frac{a}{c}\right)^2 + 0.175\left(\frac{a}{t}\right)\left(\frac{a}{c}\right) - 0.279\left(\frac{a}{c}\right)^2\right\} + \left\{1.44\left(\frac{a}{t}\right)^3 - 1.06\left(\frac{a}{t}\right)^2\left(\frac{a}{c}\right) + 0.609\left(\frac{a}{t}\right)\left(\frac{a}{c}\right)^2 - 0.249\left(\frac{a}{c}\right)^3\right\}\right] \quad (3.10)$$

$$M_b^A = 1.183 - \left\{1.22\left(\frac{a}{t}\right) + 0.286\left(\frac{a}{c}\right)\right\} + \left\{0.867\left(\frac{a}{t}\right)^2 - 0.0067\left(\frac{a}{t}\right)\left(\frac{a}{c}\right) + 0.230\left(\frac{a}{c}\right)^2\right\} + \left\{0.467\left(\frac{a}{t}\right)^3 - 1.92\left(\frac{a}{t}\right)^2\left(\frac{a}{c}\right) + 0.633\left(\frac{a}{t}\right)\left(\frac{a}{c}\right)^2 - 0.182\left(\frac{a}{c}\right)^3\right\} \quad (3.11)$$

$$M_m^B = 1.18\left\{1.0 + 0.12\left(1 - \frac{a}{2c}\right)^2\right\}\sqrt{\frac{a}{c}}\,M' \quad (3.12)$$

$$M_b^B = 1.18\left\{1.0 + 0.12\left(1 - \frac{a}{2c}\right)^2\right\}\left\{1 - 0.306\left(\frac{a}{t}\right)\right\}\sqrt{\frac{a}{c}}\,M' \quad (3.13)$$

$$M' = 0.994 - \left\{0.0126\left(\frac{a}{t}\right) - 0.0701\left(\frac{a}{c}\right)\right\} + \left\{0.0155\left(\frac{a}{t}\right)^2 + 0.179\left(\frac{a}{t}\right)\left(\frac{a}{c}\right) - 0.211\left(\frac{a}{c}\right)^2\right\} - \left\{0.0839\left(\frac{a}{t}\right)^3 - 0.231\left(\frac{a}{t}\right)^2\left(\frac{a}{c}\right) + 0.300\left(\frac{a}{t}\right)\left(\frac{a}{c}\right)^2 - 0.162\left(\frac{a}{c}\right)^3\right\} \quad (3.14)$$

$$0 \leqq a/t \leqq 0.9, \quad 0.1 \leqq a/c \leqq 1.0 \quad (3.15)$$

(4) Kawahara et al.'s equations[17]

Kawahara et al. derived the following equations using Kobayashi's results.[9]

$$M_m^A = \sum_{j=0}^{3}\sum_{j=0}^{3} C_{ij}\,(a/c)^i\,(a/t)^j \quad (3.16)$$

$$M_b^A = \sum_{i=0}^{3}\sum_{j=0}^{3} D_{ij}\,(a/c)^i\,(a/t)^j \quad (3.17)$$

$$M_b^B = \sum_{i=0}^{3}\sum_{j=0}^{3} E_{ij}\,(a/c)^i\,(a/t)^j \quad (3.18)$$

The values C_{ij}, D_{ij} and E_{ij} are given in Table 3.1. Equation (3.13) was used as M_m^B.

(5) Scott and Thorpe's equations[18]

Scott and Thorpe proposed the following equations.

$$M_m^A = M_f^A + \left(E(k)\sqrt{\frac{c}{a}} - M_f^A\right)\left(\frac{a}{t}\right)^{p^A} \tag{3.19}$$

$$M_b^A = M_f^A\left[1 - 1.36\left(\frac{a}{t}\right)\left(\frac{a}{c}\right)^{0.1}\right] \tag{3.20}$$

$$M_m^B = M_f^B + \left(E(k)\sqrt{\frac{c}{a}} - M_f^B\right)\left(\frac{a}{t}\right)^{p^B} \tag{3.21}$$

$$M_b^B = M_f^B\left(1 - 0.3\frac{a}{t}\right)\left(1 - \left(\frac{a}{t}\right)^{12}\right) + 0.394 \cdot E(k) \cdot \left(\frac{a}{t}\right)^{12}\sqrt{\frac{c}{a}} \tag{3.22}$$

in which

$$M_f^A = 1.13 - 0.07\left(\frac{a}{c}\right)^{0.5} \tag{3.23}$$

$$M_f^B = \left[1.21 - 0.1\left(\frac{a}{c}\right) + 0.1\left(\frac{a}{c}\right)^4\right]\sqrt{\frac{a}{c}} \tag{3.24}$$

$$p^A = 1.6 + 3\left(\frac{a}{c}\right)^3 + 8\left(\frac{a}{c}\right)\left(\frac{a}{t}\right)^5 + 0.008\left(\frac{a}{c}\right) \tag{3.25}$$

$$p^B = 0.3 + 1.15\left(\frac{c}{a}\right)^{1.3 \cdot a/t \cdot (a/c)^{0.2}} + 0.8\left(\frac{a}{c}\right)^3 \tag{3.26}$$

$$E(k) = \left[1 + 1.47\left(\frac{a}{c}\right)^{1.64}\right]^{0.5}$$

The stress correction factors for tension M_m^A and M_m^B, and those for bending M_b^A and M_b^B were derived from fitting Raju and Newman's results[19], and Koterazawa and Minamikawa's results[20], respectively.

(6) Newman and Raju's equations[11]

Newman and Raju performed the stress intensity factor analysis of a semi-elliptical surface crack in a finite plate shown in Fig. 3.5 with use of the finite element emthod. Wide-range equations for stress intensity factor along a crack front as a function of crack depth, crack length, plate thickness, and plate width were derived using the results obtained by the finite element analysis. The equations were expressed as follows.

$$K_I = (\sigma_m + H\sigma_b)\sqrt{\pi \frac{a}{Q}}\, F \tag{3.27}$$

in which

$$Q = 1 + 1.464\left(\frac{a}{c}\right)^{1.65} \qquad (c/a \leq 1) \tag{3.28}$$

$$F = \left[M_1 + M_2\left(\frac{a}{t}\right)^2 + M_3\left(\frac{a}{t}\right)^4\right] g f_\phi f_w \tag{3.29}$$

In eq. (3.29), M_1, M_2, M_3, f_ψ, g and f_w are given by

$$M_1 = 1.13 - 0.09\left(\frac{a}{c}\right) \tag{3.30}$$

$$M_2 = -0.54 + \frac{0.89}{0.2 + \frac{a}{c}} \tag{3.31}$$

$$M_3 = 0.5 - \frac{1.0}{0.65 + \frac{a}{c}} + 14\left(1.0 - \frac{a}{c}\right)^{24} \tag{3.32}$$

$$f_\phi = \left[\left(\frac{a}{c}\right)^2 \cos^2\phi + \sin^2\phi\right]^{1/4} \tag{3.33}$$

$$g = 1 + \left[0.1 + 0.35\left(\frac{a}{t}\right)^2\right](1 - \sin\phi)^2 \tag{3.34}$$

$$f_w = \left[\sec\left(\frac{\pi c}{2b}\right)\sqrt{\frac{a}{t}}\right]^{1/2} \tag{3.35}$$

In eq. (3.27), H is given as follows.

$$H = H_1 + (H_2 - H_1)\sin^p\phi \tag{3.36}$$

where

$$p = 0.2 + \frac{a}{c} + 0.6\frac{a}{t} \tag{3.37}$$

$$H_1 = 1 - 0.34\frac{a}{t} - 0.11\frac{a}{c}\left(\frac{a}{t}\right) \tag{3.38}$$

$$H_2 = 1 + G_1\left(\frac{a}{t}\right) + G_2\left(\frac{a}{t}\right)^2 \tag{3.39}$$

$$G_1 = -1.22 - 0.12\frac{a}{c} \tag{3.40}$$

$$G_2 = 0.55 - 1.05\left(\frac{a}{c}\right)^{0.75} + 0.47\left(\frac{a}{c}\right)^{1.5} \tag{3.41}$$

Equation (3.27) is available for $0 < a/c \leqq 1.0$, $0 \leqq a/t < 1.0$, $c/b < 0.5$ and $0 \leqq \phi \leqq \pi$.

Table 3.1 Coefficients of Polynomials proposed by Kawahara et al.

	j \ i	0	1	2	3
C_{ij}	0	1.135	− 0.211	0.190	− 0.100
	1	0.666	0.175	− 1.474	0.620
	2	0.249	− 1.671	2.295	− 0.808
	3	− 0.020	0.575	− 0.243	− 0.230
D_{ij}	0	1.138	− 0.108	− 0.043	0.031
	1	− 0.947	0.351	− 1.785	0.943
	2	1.099	− 5.187	9.268	− 5.132
	3	− 1.766	5.676	− 8.937	5.020
E_{ij}	0	0.230	1.584	− 1.022	0.462
	1	0.942	− 2.581	0.979	0.103
	2	− 0.801	1.455	1.389	− 1.996
	3	0.327	− 0.367	− 1.447	1.623

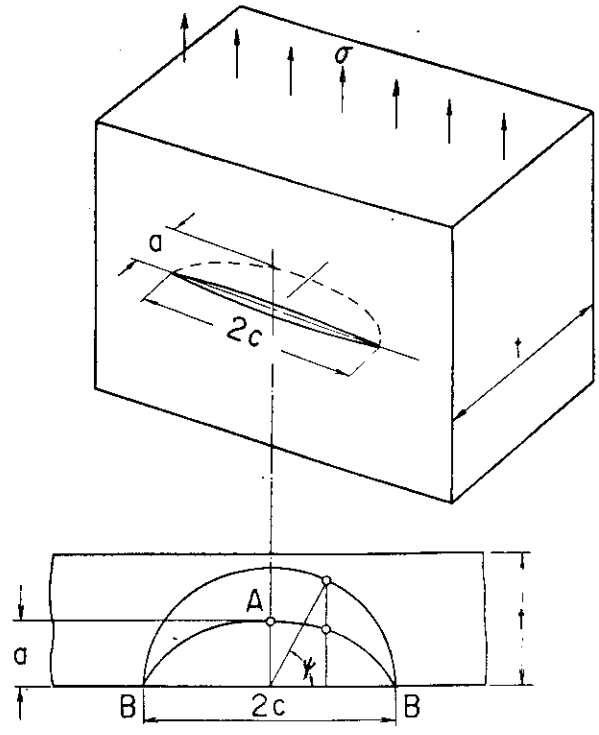

Fig. 3.1 Semi-Elliptical Crack in a plate

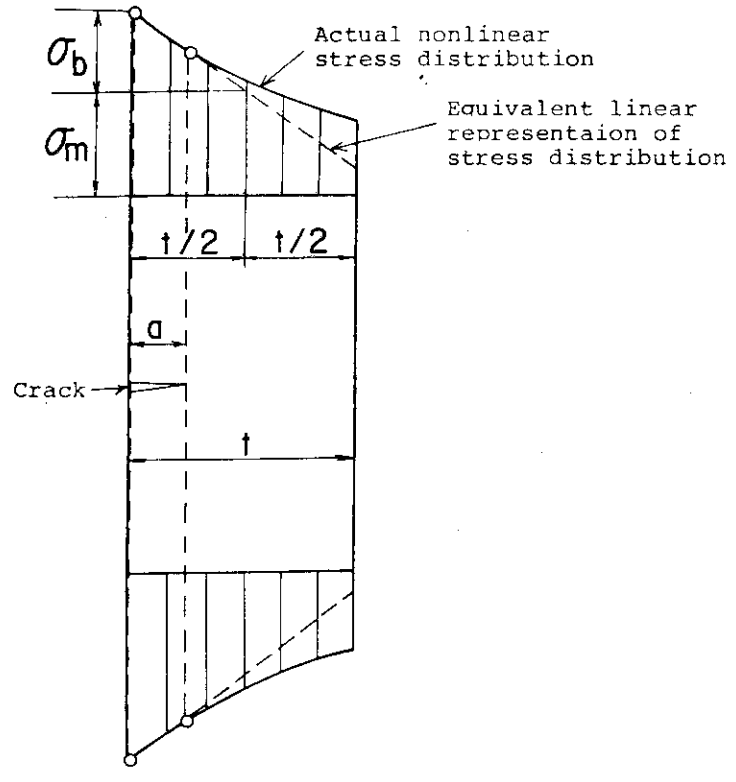

Fig. 3.2 Linearized Representation of Stresses --- ASME Boiler and Pressure Vessel Code, Sec. XI.

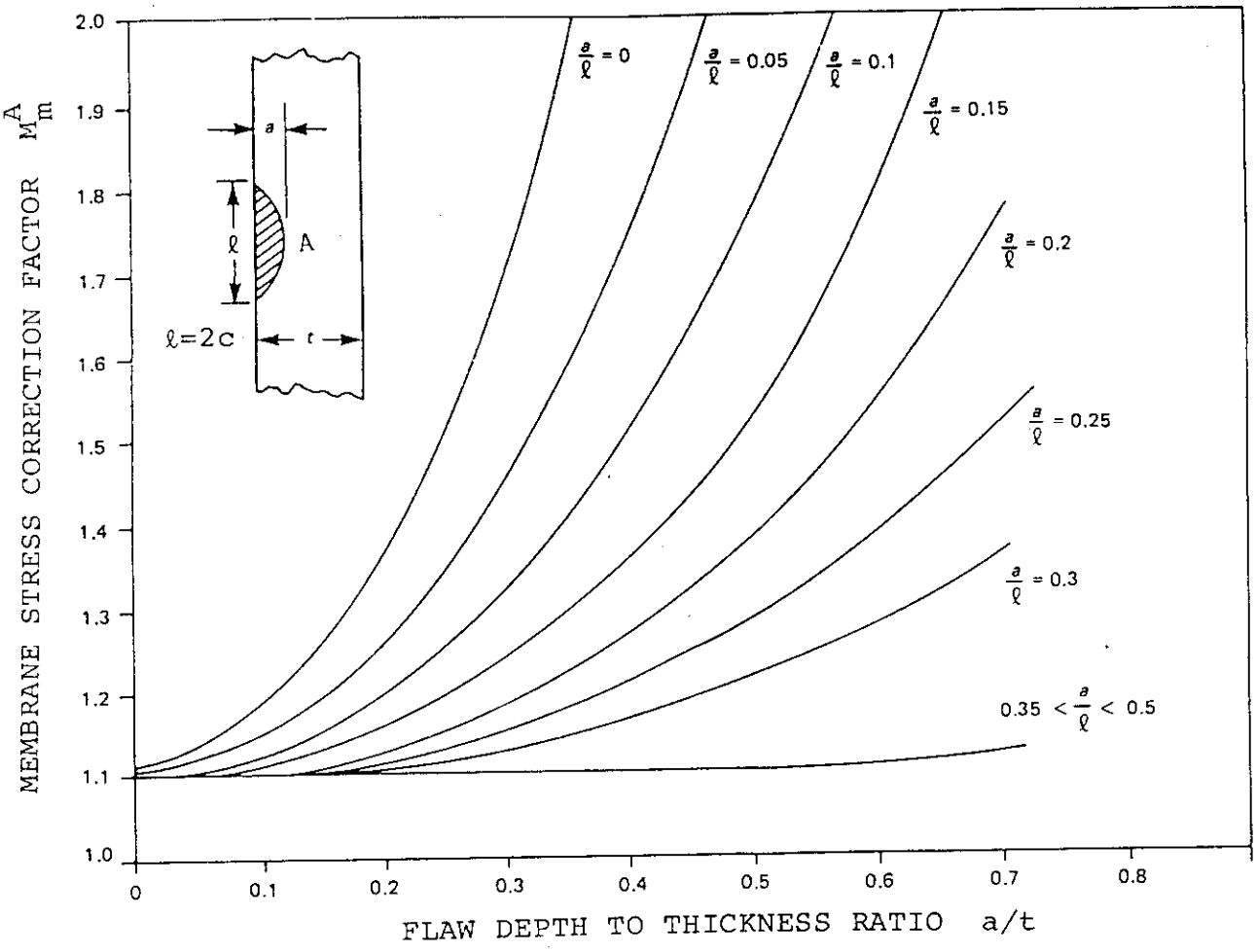

Fig. 3.3 Membrane Stress Correction Factor M_m^A for Surface Cracks --- ASME Boiler and Pressure Vessel Code, Sec. XI

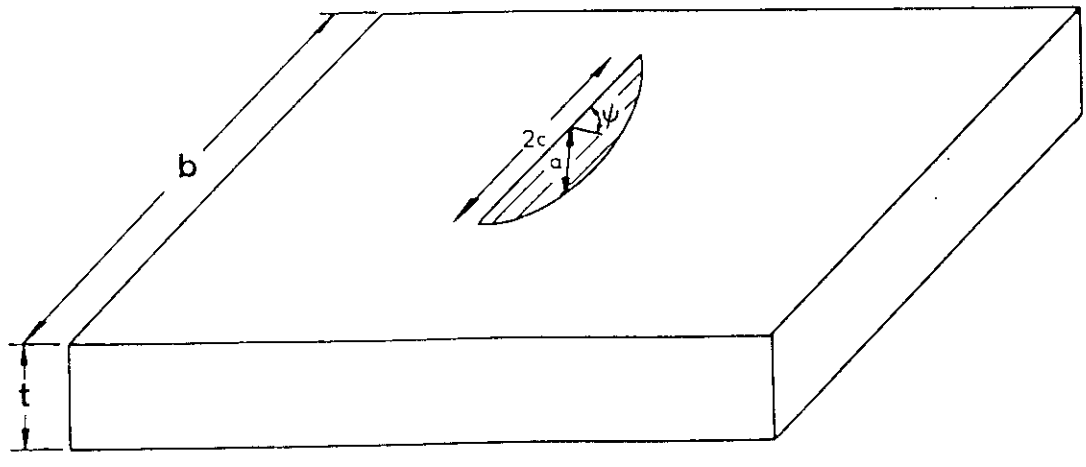

Fig. 3.5 Semi-Elliptical Crack in a Finite Plate

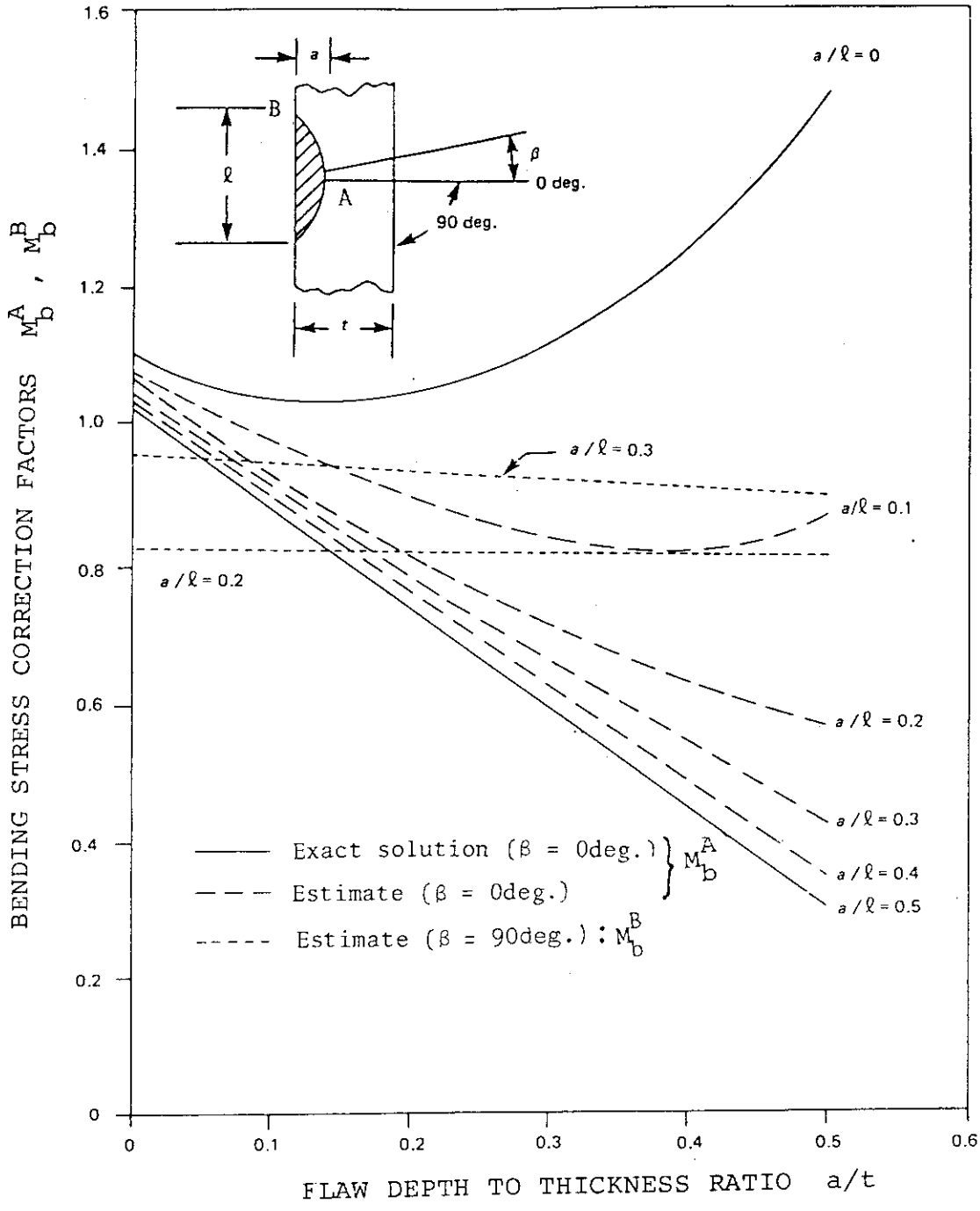

Fig. 3.4 Bending Stress Correction Factors M_b^A and M_b^B for Surface Cracks --- ASME Boiler and Pressure Vessel Code, Sec. XI

4. Numerical Results and Discussion

Some numerical results for surface cracks in three-dimensional structures are presented in this chapter. For relatively simple problems, the results of the finite element computer program EPAS-J1 were compared with the exact solution and other finite element solutions to check their accuracies. Furthermore, the stress intensity factors were compared between the finite element method and the simplified estimation methods for surface cracks in complex structures.

4.1 Embedded circular crack and semi-circular crack in a plate under uniform tension

The results are shown for an embedded circular crack and a semi-circular crack in a plate under uniform tension. Figure 4.1 shows an eighth region for an embedded circular crack problem or a quarter region for a semi-circular crack problem. The face ABCD is a surface of symmetry face for an embedded circular crack problem, while this face is a free for a semi-circular crack problem. Figure 4.2 shows the finite element meshes used in the analysis by EPAS-J1. The 16-node solid elements were used in the whole region.
ments were used in the whole region.

Table 4.1 shows the results of an embedded circular crack problem obtained by EPAS-J1. These results were compared with the exact solution for an embedded crack in an infinite plate. The results obtained by EPAS-J1 agreed with the exact solution within one percent.

Figure 4.3 shows the distribution of stress intensity factor for a semi-circular crack in a plate. Other finite element solutions are also depicted in the figure for comparison. Ando et al.[21] obtined the stress intensity factor from the J-integral value calculated by path integral. Newman and Raju[11] used nodal-force method. Yagawa and Nishioka[22] applied a superposition of the analytical and the finite element solutions to surface crack problems. Yagawa et al.[23] proposed the method based on the discretization error of the finite element technique and obtained the accurate stress intersity factor. Figure 4.3 shows that the present result obtained by EPAS-J1 is in good agreement with other finite element solutions.

4.2 Semi-elliptical crack in the inner surface of a pressurized cylinder

Figure 4.4 shows a pressurized cylinder with a longitudinal semi-elliptical crack. The dimensions of the cylinder and crack, and Possion's ratio ν used in the analysis are as follows.

$R_o/R_i = 1.5$, $a/c = 0.6$, $a/(R_o - R_i) = 0.4$, $\nu = 0.3$

Figure 4.5 shows the analytical model of a quarter of the cylinder used in the analysis by EPAS-J1. The 16-node solid elements were used in the neighborhood of the crack and the remainder of the cylinder was modeled by the 4-node thin shell elements. Figures 4.6 and 4.7 show the finite element meshes of the total structure and the surface with a crack, respectively. The exact solution for circumferential stress $\sigma_{\theta\theta}$ normal to a crack surface was used to apply the simplified estimation methods mentioned in Chapter 3 to the present problem. It is given as follows:

$$\sigma_{\theta\theta} = \frac{k^2/R^2+1}{k^2-1} P_i \qquad k = \frac{R_o}{R_i} \qquad R = \frac{r}{R_i} \tag{4.1}$$

in which r denoetes the radial coordinate. According to the procedure shown in Fig. 3.2, the stress $\sigma_{\theta\theta}$ is separated into the membrane component σ_m and the bending component σ_b. Then the stress intensity factors can be calculated using eqs. (3.1) and (3.2) and applying appropriate stress correction factors.

Table 4.2 shows the comparison of the stress intensity factors at $\psi=0°$ and $\psi=90°$ obtained by EPAS-J1 and those calculated using the simplified estimation methods. The results are mormalized by the following closed form solution K_0 for an elliptical crack embedded in an infinite body subjected to a uniform tension stress σ_0:

$$K_o = \frac{\sigma_o \sqrt{\pi}}{E(k)} \sqrt{a/c} (c^2 \sin^2\phi + a^2 \cos^2\phi)^{\frac{1}{4}} \tag{4.2}$$

in which

$$\sigma_0 = \frac{2 R_i^2}{R_o^2 - R_i^2} P_i \tag{4.3}$$

Compared with the present results obtained by EPAS-J1, the simplified estimation emthod using Scott and Thorpe's equations gives good result at the surface point, $\psi=0°$, and the simplified estimation method using Soya et al.'s equation gives fairly good result at the deepest point, $\psi=90°$.

Fig. 4.8 shows the distribution of the nondimensional stress intensity factor along a crack front. Other results are also depicted in the figure for comparison. Atluri and Kathiresan[24] used the special element containing the singularity of stress around a crack tip and the hybrid displacement technique to ensure the continuity of the displacement between the special and the conventional elements. In this method the stress intensity factor can be solved directly along with the unknown nodal displacements. Blackburn and Hellen[25] utilized the virtual crack extension method. Kobayashi et al.[26] obtained the stress intensity factor by applying the curvature correction to that of a surface crack in a flat plate. Newman and Raju's solution indicates the results obtained by the simplified estimation method using Newman and Raju's equations for the stress intensity factor. Nishioka and Atluri[27] used an alternative method which was the combination of the finite element method and an analytical solution for an elliptical crack in an infinite solid. The present result obtained by EPAS-J1 agrees well with Atluri and Kathiresan's solution near the surface of the cylinder, and with Nishioka and Atluri's solution in the remainder of the region. The simplified estimation method using Newman and Raju's equations provides larger stress intensity factor than any other solutions shown in Fig. 4.8 except near the outer surface of the cylinder.

4.3 Ellipse-shaped cracks in the inner surface of a cylinder subjected to shear force

Figure 4.9 shows a cylinder subjected to shear force F. A surface crack was assumed to be contained in the fixed end A-A' where the displacement of z-component was fixed but the deformation in the x-y plane was not constrained. Three types of ellipse-shaped surface cracks ST-1 through ST-3 were considered in the analysis.

Fig. 4.10 shows the analytical model of a half of the cylinder used in the analysis by EPAS-J1. The 16-node solid elements were allocated in the neighborhood of a crack, while the shell and beam elements were used to model the remainder of the cylinder. The above modeling was employed due to the reasons that the region near the surface crack was governed by the three-dimensional stress field and that the whole deformation of the cylinder could be represented by the beam type

simplification. Figure 4.11 shows the finite element meshes in the surface with a crack for ST-1 through ST-3.

In order to apply the simplified estimation methods to the present problem, the stress at the fixed end of the cylinder was calculated by the elementary beam theory and the stress distribution along the line A-A' was used to obtain σ_m and σ_b according to the method shown in Fig. 3.2. In the simplified estimation methods, a surface crack assumed to be semi-elliptical shape.

Table 4.3 shows the comparison of stress intensity factor at $\psi=0°$ and $\psi=90°$ obtained by EPAS-J1 and those calculated using the simplified estimation methods. A large difference can be found in the stress intensity factors at the surface point ($\psi=0°$) between the finite element method and the simplified estimation emthods, especially in the case of deep and large crack such as ST-3.

Figure 4.12 shows the distributions of the stress intensity factors along a crack front. It is found from the figure that the results obtained by the simplified estimation method using Newman and Raju's equations are larger than the finite element solutions near the surface point, $\psi=0°$, especially in the case of ST-3. This is bacause the stress is overestimated in the neighborhood of the surface point in the simplified estimation method owing to neglecting the circumferential distribution of stress.

4.4 Interacting effect of multiple surface cracks

Figures 4.13 and 4.14 show a plate with three semi-circular cracks subjected to tension σ_m and bending σ_b and a cylinder with three circular shaped cracks subjected to shear force F, respectively. The plate has three cracks of the same shape and the same distance between the cracks as the cylinder. The tensile stress σ_m and bending stress σ_b applying the plate were determined by the stress distribution on the line A-A' of the cylinder calculated from the elementary beam theory. Figures 4.15 and 4.16 show the analytical models for the plate and the cylinder, respectively. The finite element meshes are presented in Fig. 4.17 for the plate and in Fig. 4.18 for the cylinder. Figures 4.19 and 4.20 show the finite element meshes in the surfaces with cracks. As shown in Figs. 4.19 and 4.20, the single crack model was analyzed using the

same finite element meshes as the three crack model in order to clarify the interacting effect of multiple cracks.

Table 4.4 shows the comparison of the stress intensity factors for a semi-circuler crack in a plate. Figure 4.21 shows the comparison of the distributions of the stress intensity factors along a crack front between the finite element method and the simplified estimation method using Newman and Raju equations. The finite element solutions are smaller at the deepest point (ψ=90°) and larger at the surface point (ψ=0°) than other solutions.

Figures 4.22 and 4.23 show the distributions of stress intensity factors for multiple cracks in a plate and cylinder, respectively. The results for single crack are also given in these figures for comparison. The intenacting effect of multiple cracks can be seen by comparing the results of multiple cracks with those of single crack. The interating effect of multiple cracks is given in Fig. 4.24 where the magnification factor F is defined as

$$F = \frac{\text{The stress intensity factor for Crack No.1 in multiple cracks}}{\text{The stress intensity factor for single crack}}$$

F_A in the figure indicates the magnification factor at the point of A in the two-dimensional multiple cracks shown in Fig. 4.25. F_A is given as follows.[27]

$$F_A = \left(\frac{(1+\lambda_2)^2-\lambda_1^2}{(1-\lambda_2)^2-\lambda_1^2}\right)^{\frac{1}{2}} \cdot \frac{E(m_3)}{K(m_3)} \tag{4.4}$$

in which

$$m_3 = 2\left(\frac{\lambda_2}{(1+\lambda_2)^2-\lambda_1^2}\right)^{\frac{1}{2}}, \qquad \lambda_1=\frac{a_1}{d}, \qquad \lambda_2=\frac{a_2}{d} \tag{4.5}$$

$K(m_3)$ = complete ellpitic integral of first kind

$E(m_3)$ = complete elliptic integral of second kind

As pointed out by others[28][29], Fig. 4.24 shows that the interacting effect of multiple surface cracks is smaller than that of two dimensional multiple cracks. It is also found that the multiple cracks in a plate shows the larger interacting effect than those in a cylinder.

4.5 Ellipse-shaped cracks in the inner surface of elbow subjected to in-plane bending

Figure 4.26 shows a bend pipe subjected to in-plane bending. Two ellipse-shaped cracks were assumed to exsist at 0° and 180° in the center of an elbow along the longitudinal direction. As shown in Fig. 4.27, a small crack EL-1 and a large crack EL-2 were considered in the analysis. The stress analysis of uncracked model EL-0 was performed to obtain the stress distribution which was used in the simplified estimation methods described in Chapter 3. Figure 4.28 shows the analytical models for EL-0 through EL-2. In all cases, the beam elements were used to model a straight pipe. In order ot model an elbow, only the thick shell elements were used in the uncrackde model EL-0, while both the solid elements and the thick shell elements were used in the cracked models EL-1 and EL-2. Figure 4.29 shows the finite element meshes for EL-0 through EL-2. The finite element meshes in the surface with a crack are shown in Fig. 4.29 for EL-1 and EL-2. Figures 4.31 and 4.32 show the distributions of the axial stress σ_θ and the circumferential stress σ_ϕ in the cross section at the center of an elbow for the uncracked model EL-0. The experimental data[30] and the results obtained from the following equations given in ASME Boiler and Pressure Vessel Code, Sec. III, NB 3685. 1-2, are depicted in those figures for comparison.

$$\sigma_\theta = \frac{M}{Z}\left(\sigma_{tm} \pm \nu \sigma_{nb}\right) \qquad \text{(+: outside, -: inside)} \tag{4.6}$$

$$\sigma_\varphi = \frac{M}{Z}\left(\nu t_m \pm \sigma_{nb}\right) \qquad \text{(+: outside, -: inside)} \tag{4.7}$$

$$\sigma_{tm} = \sin\varphi + \{(1.5\,X_2 - 18.75\sin 3\varphi + 11.25\sin 5\varphi\} / X_4 \tag{4.8}$$

$$\sigma_{nb} = \lambda(9\,X_2\cos 2\varphi + 2.25\cos 4\varphi) / X_4 \tag{4.9}$$

$$\lambda = tR / r^2\sqrt{1-\nu^2} \tag{4.10}$$

$$X_1 = 5 + 6\lambda^2 \tag{4.11}$$

$$X_2 = 17 + 600\lambda^2 \tag{4.12}$$

$$X_3 = X_1 X_2 - 6.25 \tag{4.13}$$

$$X_4 = (1-\nu^2)(X_3 - 4.5\,X_2) \tag{4.14}$$

Z = section modulus of cross section

r = mean cross section radius

The finite element solutions using the thick shell elements agree well with experimental data. The distribution of σ_ϕ through thickness at ϕ=90° was used to obtain the membrane stress component σ_m and the bending stress component σ_b shown in Fig. 3.2 which were required for the application of the simplified estimation methods.

Table 4.5 shows the comparison of the stress intensity factors at ψ=0° and ψ=90°obtained by EPAS-J1 and those calculated using the simplified estimation methods. The present results obtained by EPAS-J1 are in fairly good agreement with those obtained by the simplified estimation method using Scott and Thorpe's equations for a small crack model EL-1 and with those obtained by the simplified estimation method using Newmen and Raju's equations for a large crack model EL-2

Figure 4.33 shows the distributions of the stress intensity factor along a crack front obtained by the finite element method and the simplified estimation method using Newman and Raju's equations. For a small crack, a good agreement is found between both results. For a large crack, the simplified estimation method using Newman and Raju's equations provides larger stress intensity factor than the finite element emthod, especially in the region from 20° to 60°.

Table 4.1 Stress Intensity Factors for an Embedded circular crack in a Plate

ϕ	K_I	$K_I / 2\sigma_0\sqrt{a/\pi}$
0°	1.610319	1.00912
15°	1.610880	1.00947
30°	1.606658	1.00682
45°	1.602094	1.00396
60°	1.603150	1.00463
75°	1.603036	1.00455
82.5°	1.603063	1.00457
90°	1.603231	1.00468

$2\sigma_0\sqrt{a/\pi}$ = the exact solution for an embedded crack in an infinite plate

Table 4.2 Comparison of Nondimensional Stress Intensity Factors for a Semi-Elliptical Crack in Inner Surface of a Pressurized Cylinder

	Nondimensional Stress Intensity Factor , F	
	ϕ	
	0°	90°
Present	1.585	1.278
ASME Sec.XI		1.452
Sakakibara.et al.(*)	1.500 (1.578)	1.379 (1.451)
Soya,et al.	1.452	1.241
Kawahara,et al.	1.465	1.441
Scott & Thorpe	1.583	1.382
Newman & Raju	1.506	1.397

(*) The numerals in the parentheses indicate the stress intensity factors multiplied by the curvature correction factor.

Table 4.3 Comparison of Stress Intensity Factors for an Ellipse-Shaped Crack in Inner Surface of a Cylinder Subjected to Shear Force

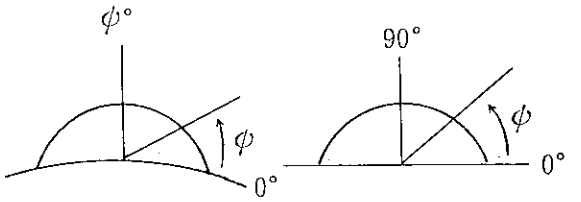

	Stress Intensity Factor, K_I (MPa · $m^{1/2}$)					
	ST−1 (a=8mm, c=12mm)		ST−2 (a=18mm, c=20mm)		ST−3 (a=32mm, c=75mm)	
	φ		φ		φ	
	0°	φ_0° or 90°	0°	φ_0° or 90°	0°	φ_0° or 90°
Present	10.81	13.61	17.31	18.31	20.03	45.72
ASME Sec. XI		14.19		19.67		
Sakakibara, et al.(*)	13.65 (13.72)	14.19 (14.25)	21.34 (22.05)	19.66 (20.31)		
Soya, et al.	12.48	13.48	19.30	18.29	24.73	65.01
Kawahara, et al.	12.54	14.06	19.37	19.30	24.27	50.58
Scott & Thorpe	12.32	13.81	20.66	19.53	46.28	50.23
Newman & Raju	12.37	13.92	21.01	19.74	40.40	48.57

1 MPa · $m^{1/2}$ = 3.225 kgf · $mm^{-3/2}$

(*) The numerals in the parentheses indicate the stress intensity factors multiplied by the curvature correction factor.

Table 4.4 Comparison of Stress Intensity Factors for a Semi-Circular Crack in a Plate Subjected to Tensile and Bending Forces

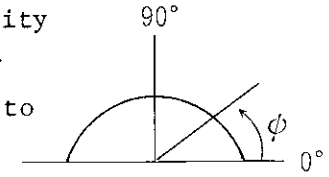

	Stress Intensity Factor K_I (MPa • $m^{1/2}$)	
	φ	
	0°	90°
Present	26.01	20.11
ASME Sec. XI		21.57
Sakakibara, et al.	23.86	21.18
Soya, et al.	21.53	19.94
Kawahara, et al.	21.64	20.26
Scott & Thorpe	24.82	22.17
Newman & Raju	24.81	21.54

1 MPa • $m^{1/2}$ = 3.225 Kgf • $mm^{-3/2}$

Table 4.5 Comparison of Stress Intensity Factors for Ellipse-Shaped Cracks in Inner Surface of an Elbow Subjected to In-Plane Bending

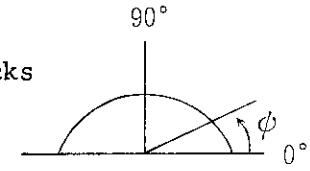

	Stress Intensity Factor, K_I (MPa • $m^{1/2}$)			
	EL-1 (a = 8 mm, c = 24 mm)		EL-2 (a = 22.2 mm, c = 40.85 mm)	
	φ		φ	
	0°	90°	0°	90°
Present	24.81	22.40	44.22	23.81
ASME Sec. XI		22.27		27.07
Sakakibara, et al.(*)	23.57 (23.68)	22.38 (22.49)	42.46 (47.77)	25.35 (28.53)
Soya, et al.	27.33	24.19	41.24	30.12
Kawahara, et al.	26.39	23.62	41.86	26.60
Scott & Thorpe	25.72	22.69	39.67	21.74
Newman & Raju	26.26	23.64	47.12	25.15

1 MPa • $m^{1/2}$ = 3.225 Kgf • $mm^{-3/2}$

(*) The numerals in the parentheses indicate the stress intensity factors multiplied by the curvature correction factor.

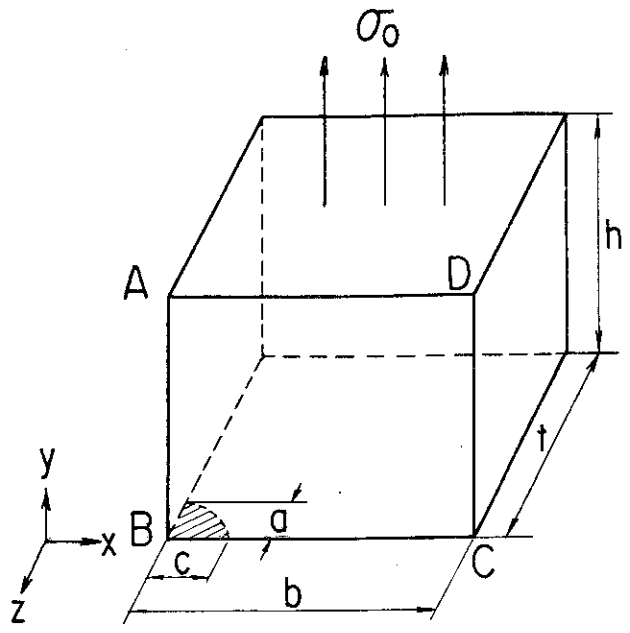

a/c = 1.0 h/b = 1.0

c/b = 0.2 b/t = 1.0

Fig. 4.1 Embedded Circular Crack or Semi-Circular Crack in a Plate Subjected to Tensile Force

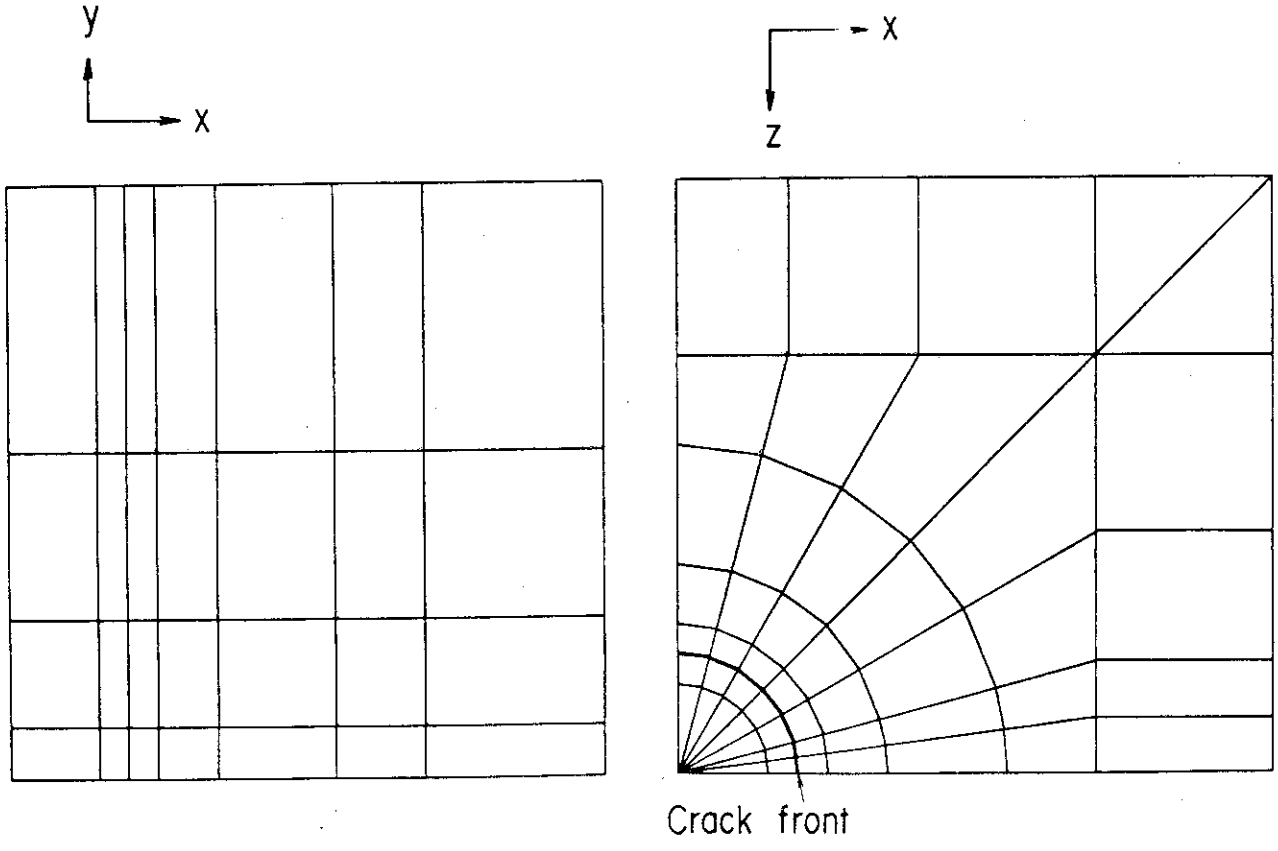

Fig. 4.2 Finite Element Meshes for an Embedded Circular Crack or Semi-Circular Crack in a Plate Subjected to Tensile Force

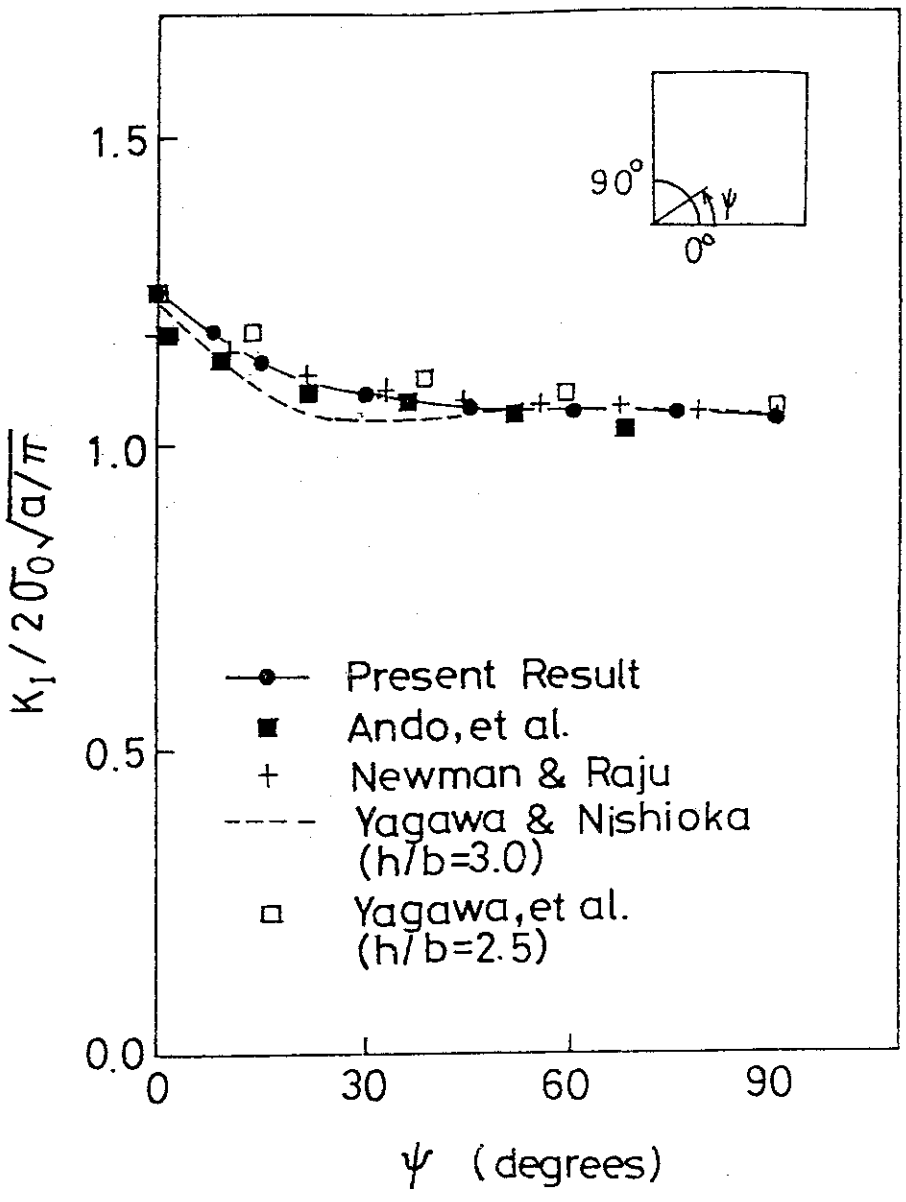

Fig. 4.3 Distribution of Stress Intensity Factors for a Semi-Circular Crack in a Plate Subjected to Tensile Force

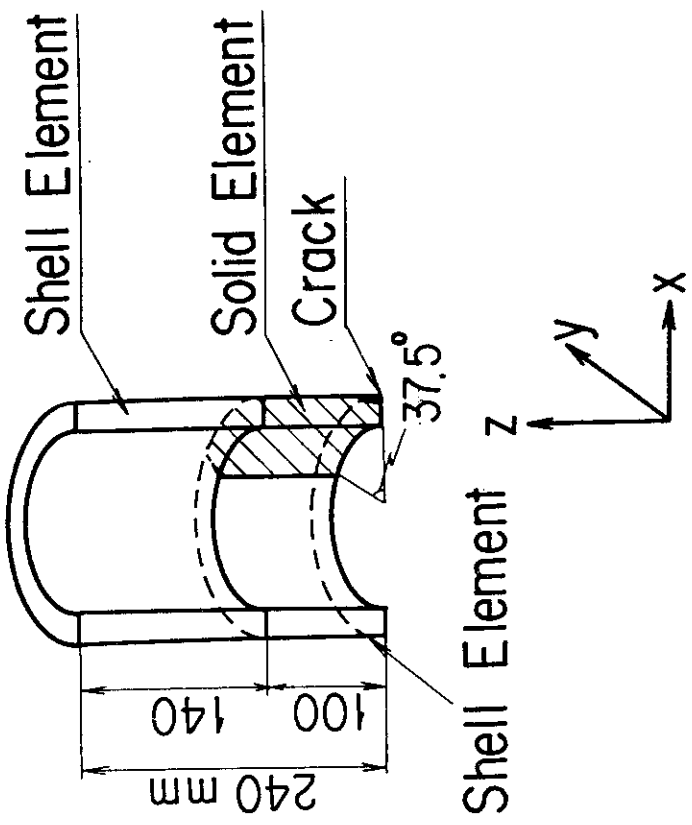

Fig. 4.5 Analytical Model for a Pressurized Cylinder with a Semi-Elliptical Crack

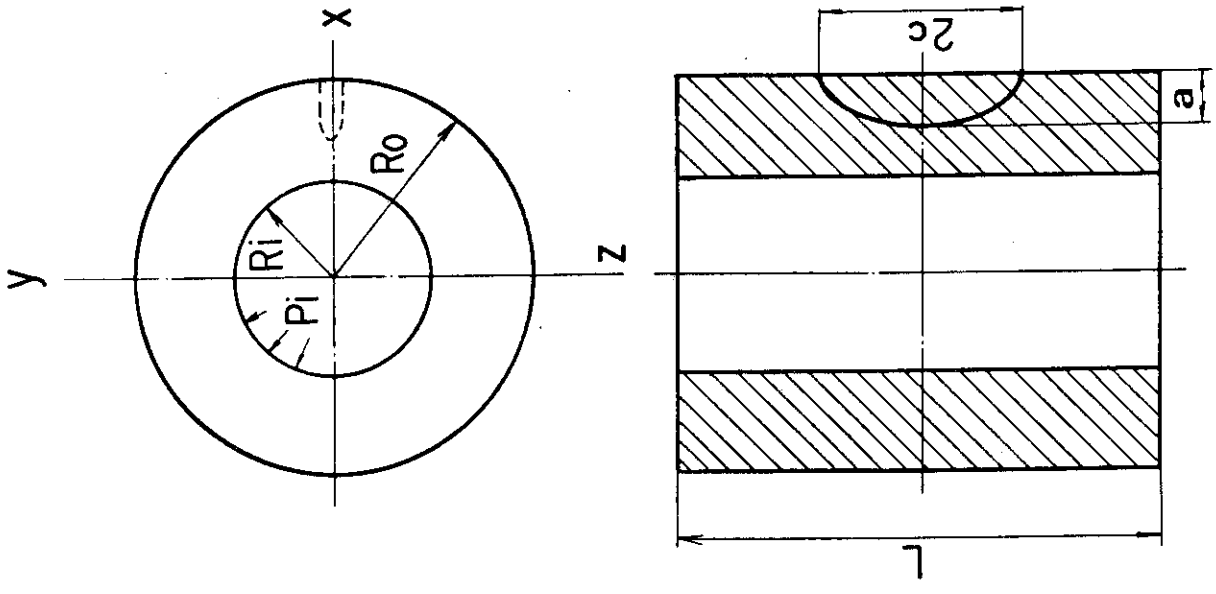

Fig. 4.4 Pressurized Cylinder with a Semi-Elliptical Crack

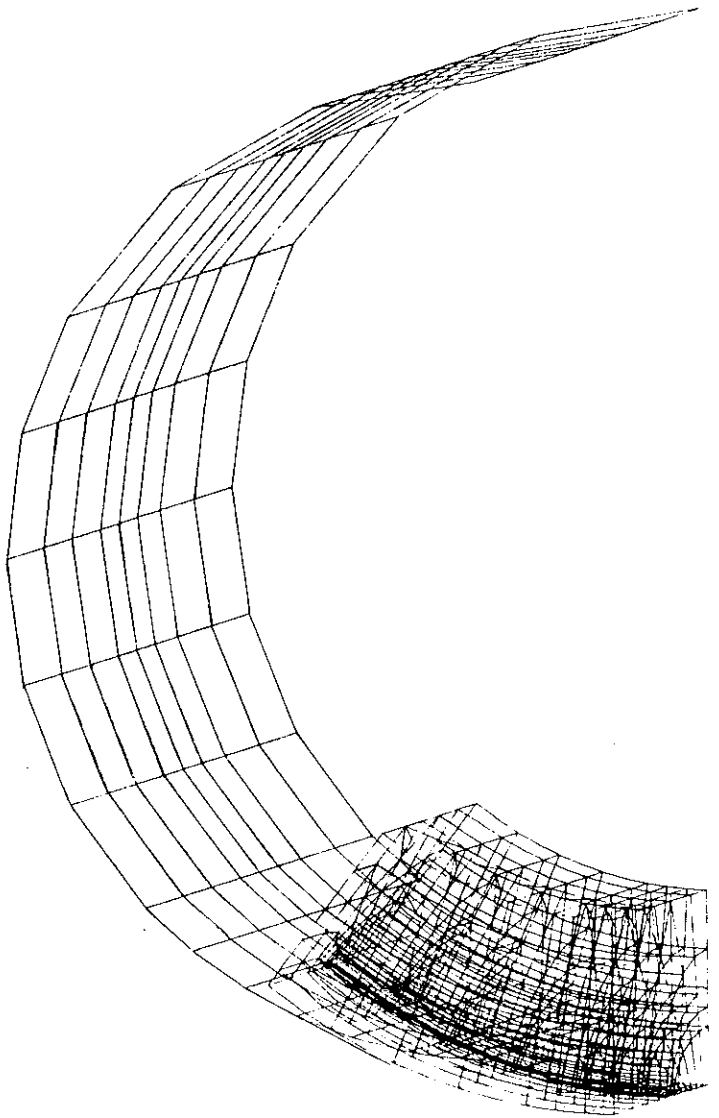

Fig. 4.6 Finite Element Mesh for a Pressurized Cylinder with a Semi-Elliptical Crack

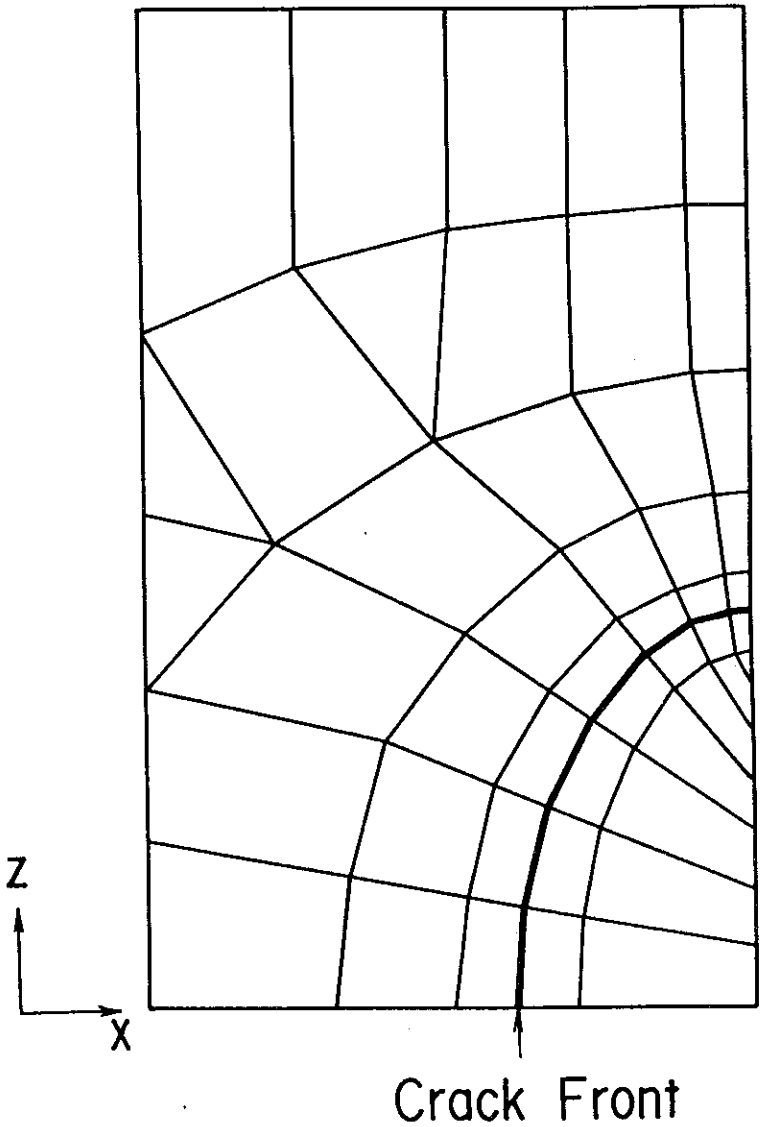

Fig. 4.7 Finite Element Mesh in the Surface with a Crack

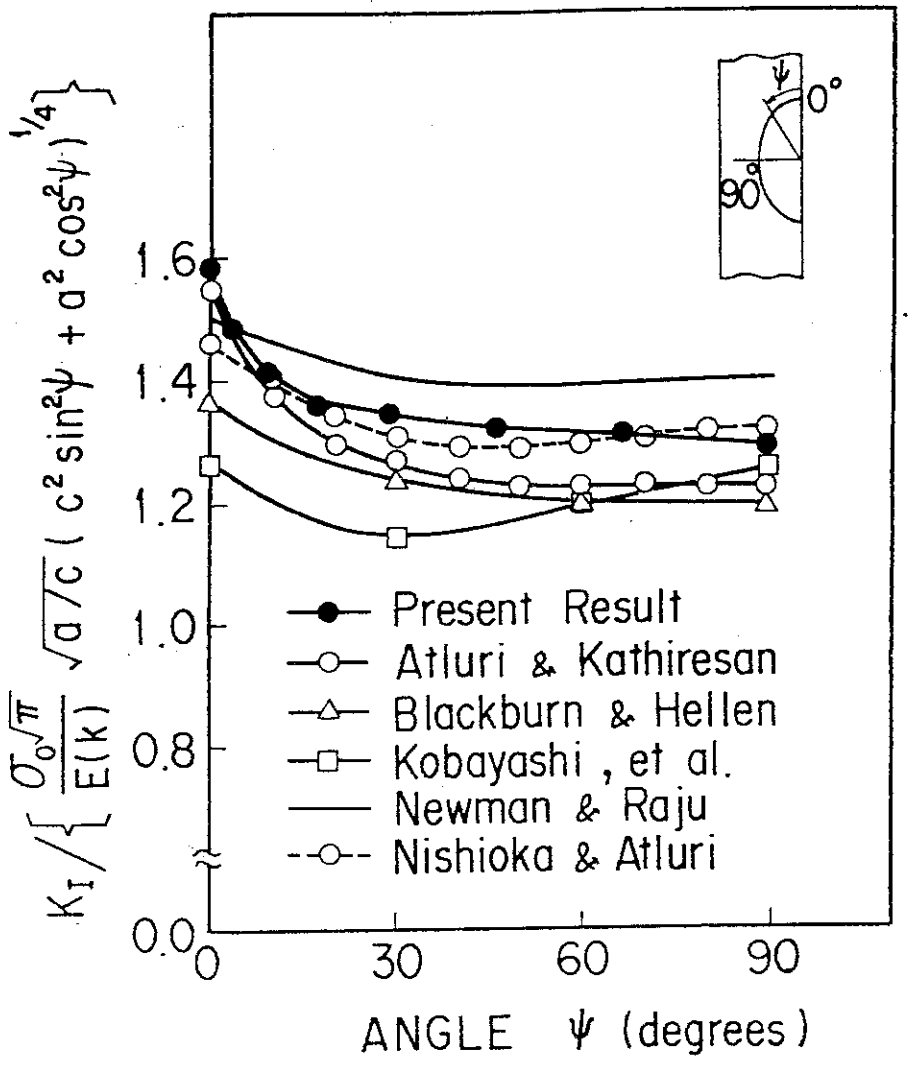

Fig. 4.8 Distribution of Nondimensional Stress Intensity Factors for a Semi-Elliptical Crack in Inner Surface of a Pressurized Cylinder

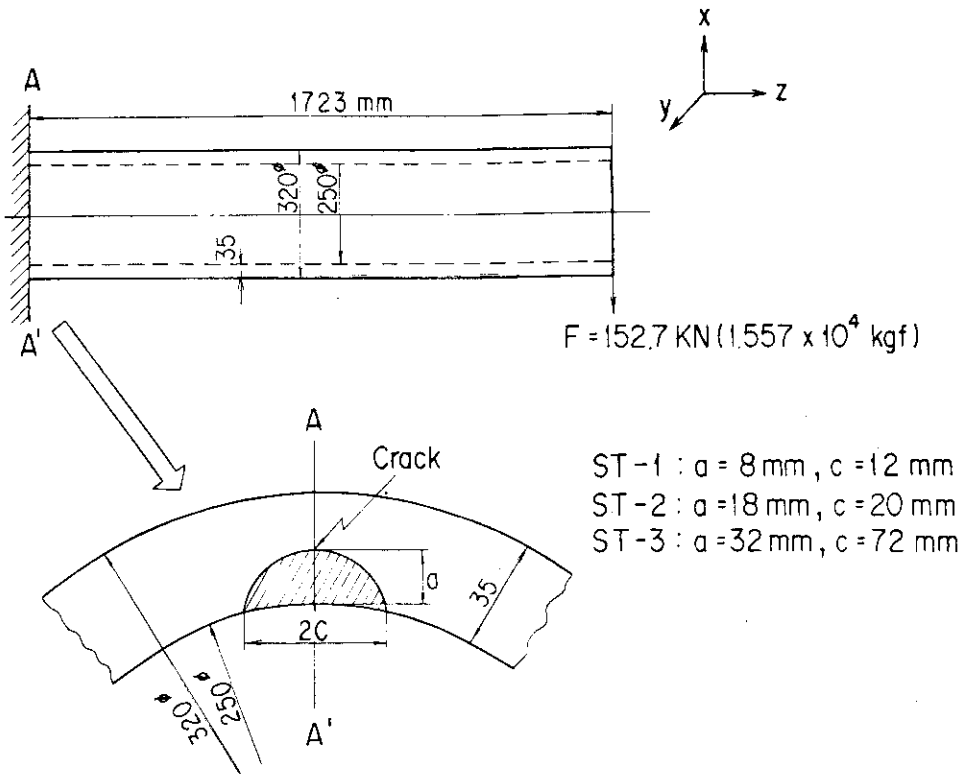

Fig. 4.9 Cylinder with an Ellipse-Shaped Crack Subjected to Shear Force

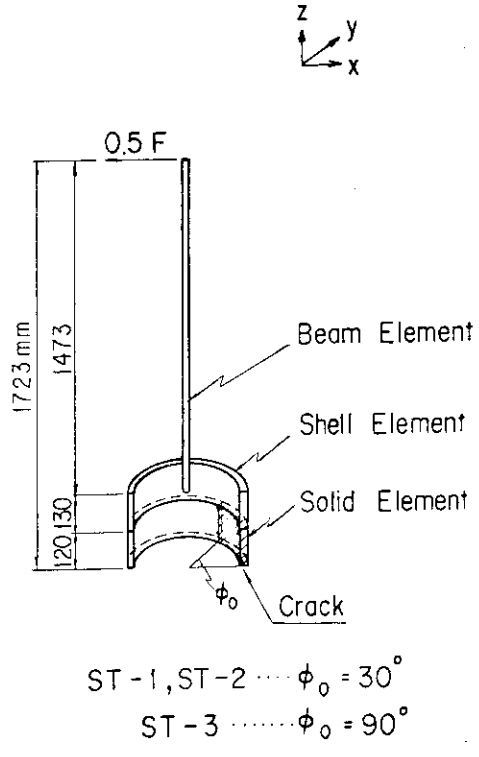

Fig. 4.10 Analytical Model for a Cylinder with an Ellipse-Shaped Crack Subjected to Shear Force

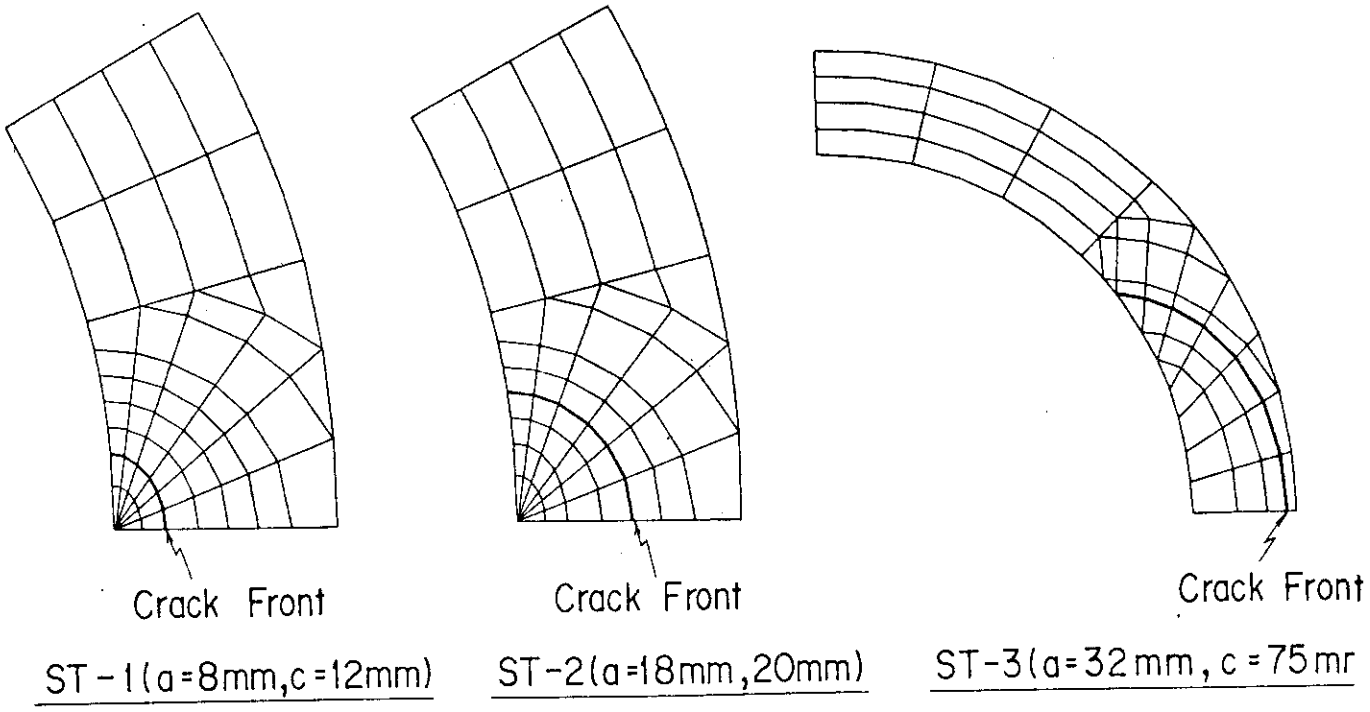

Fig. 4.11 Finite Element Meshes in the Surface with a Crack

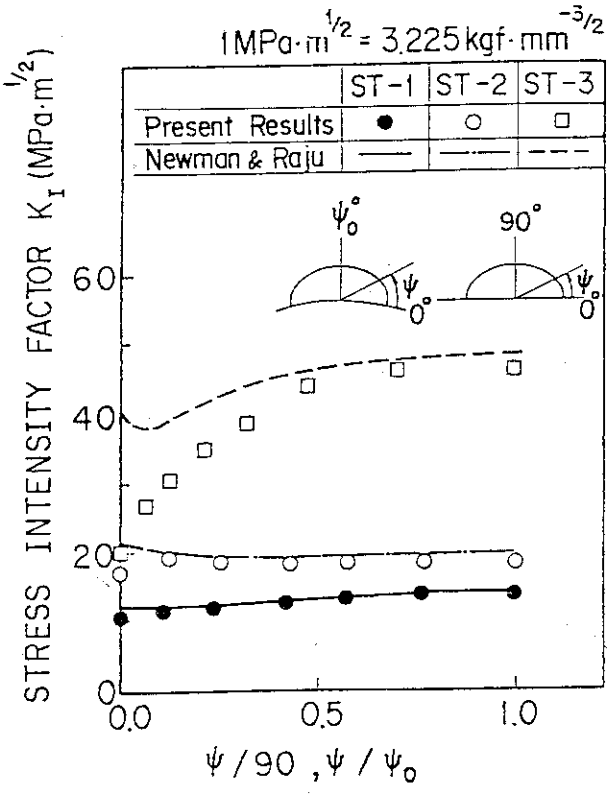

Fig. 4.12 Distribution of Stress Intensity Factors for an Ellipse-Shaped Crack in Inner Surface of a Cylinder Subjected to Shear Force

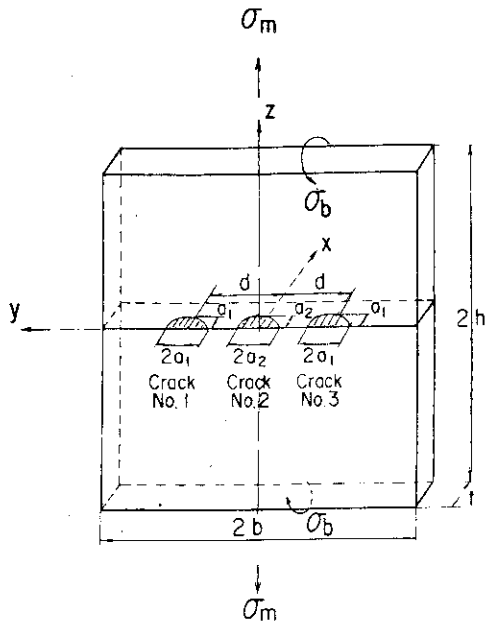

a_1 = 19.6 mm , a_2 = 22.2 mm , b = 111 mm ,
d = 50 mm , h = 350 mm ,
σ_m = 116.11 MPa (11.84 kgf/mm^2)
σ_b = 14.22 MPa (1.45 kgf/mm^2)

Fig. 4.13 Plate with Three Semi-Circular Cracks Subjected to Tensile and Bending Forces

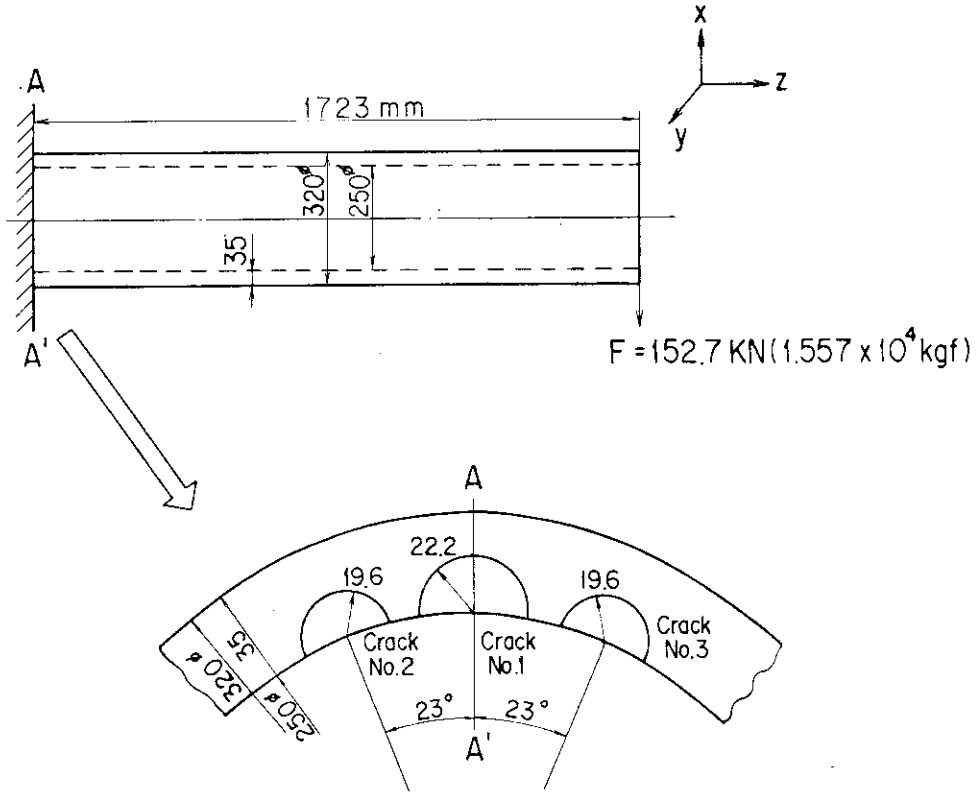

Fig. 4.14 Cylinder with Three Circle-Shaped Cracks Subjected to Shear Force

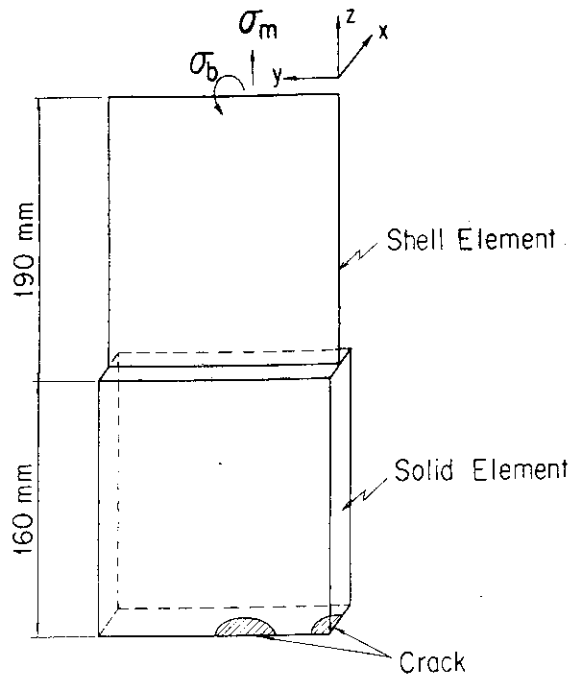

Fig. 4.15 Analytical Model for a Plate with Three Semi-Circular Cracks Subjected to Tensile and Bending Forces

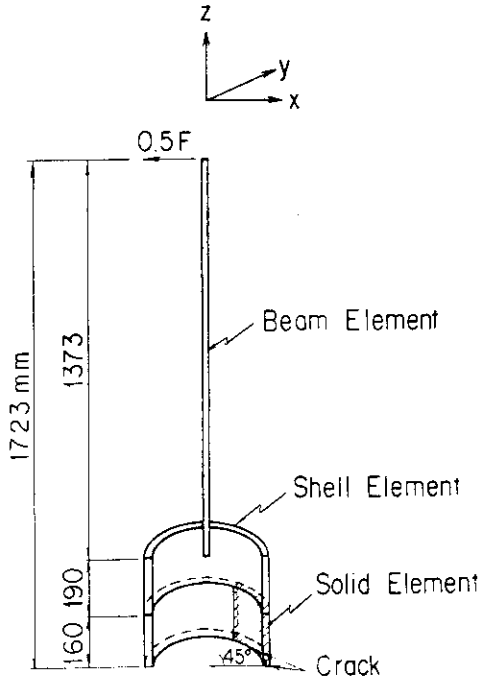

Fig. 4.16 Analytical Model for a Cylinder with Three Circle-Shaped Cracks Subjected to Shear Force

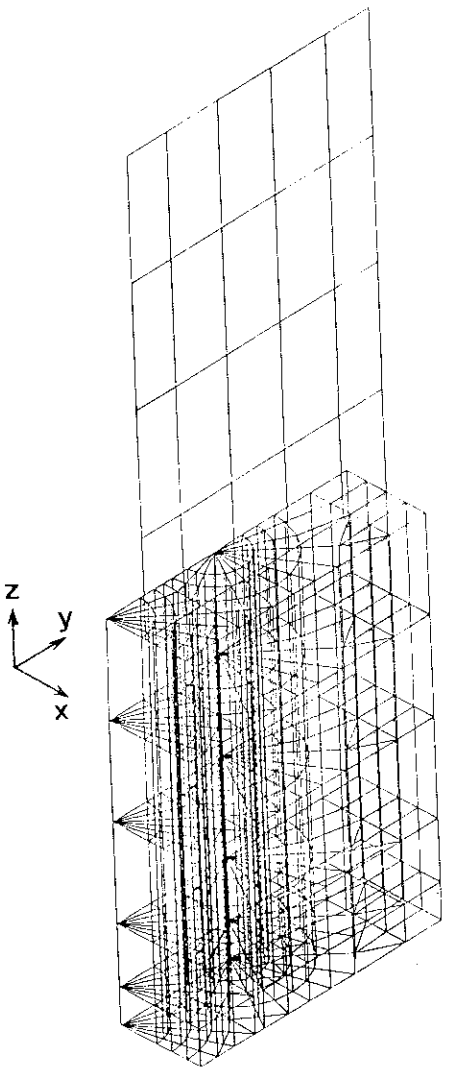

Fig.4.17 Finite Element Mesh for a Plate with Three Semi-Circular Cracks Subjected to Tensile and Bending Forces

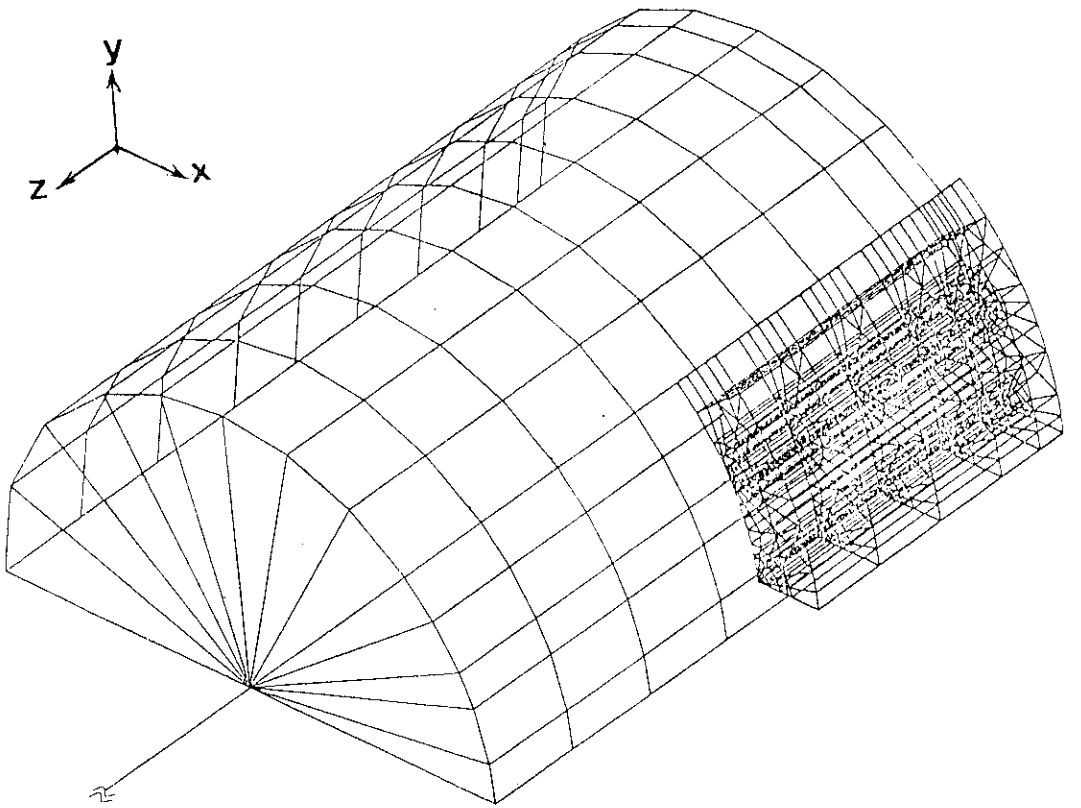

Fig.4.18 Finite Element Mesh for a Cylinder with Three Circle-Shaped Cracks Subjected to Shear Force

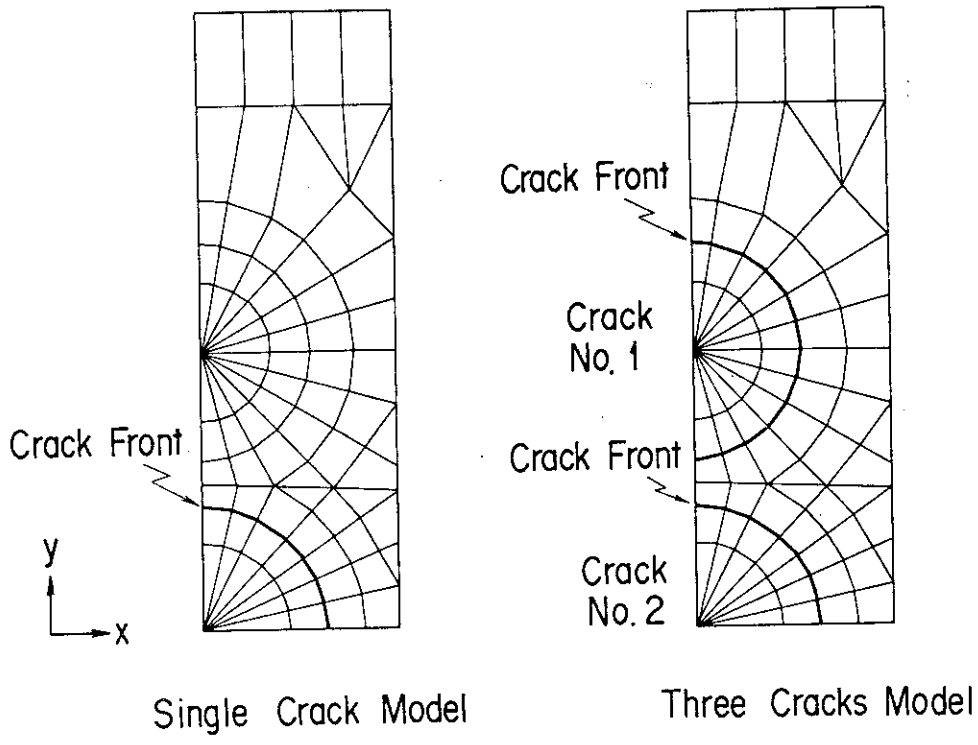

Fig. 4.19 Finite Element Meshes in the Surfaces with Cracks --- Plate

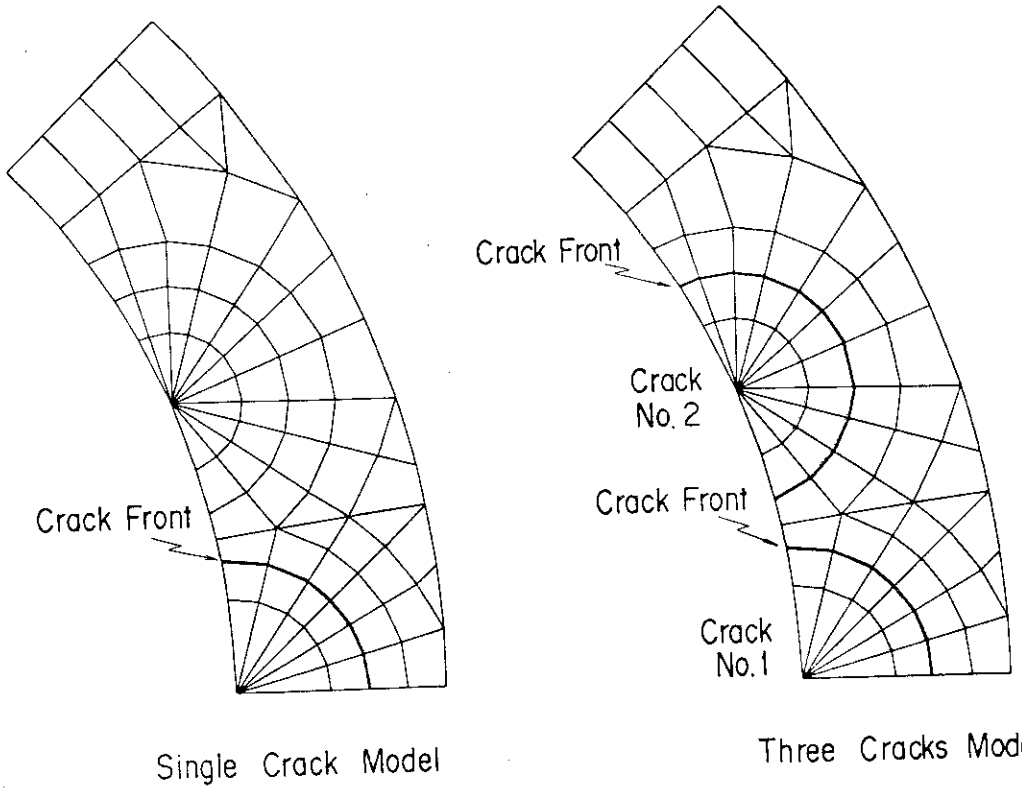

Fig. 4.20 Finite Element Meshes in the Surfaces with Cracks --- Cylinder

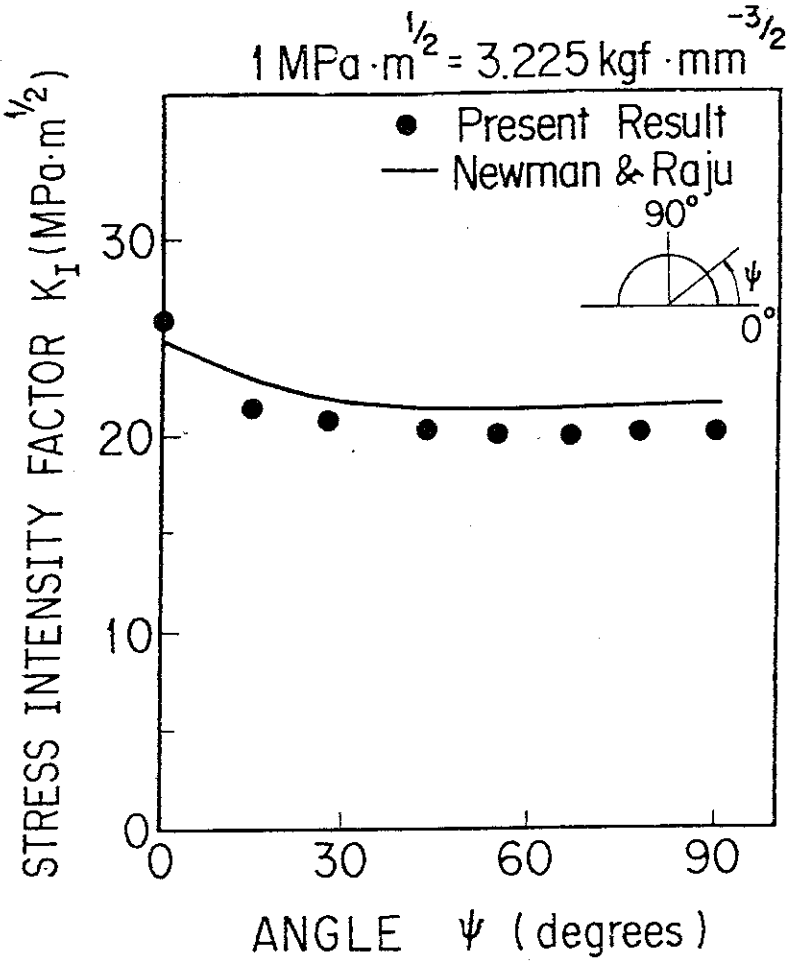

Fig. 4.21 Distribution of Stress Intensity Factors for Single Semi-Circular Crack in a Plate Subjected to Tensile and Bending Forces

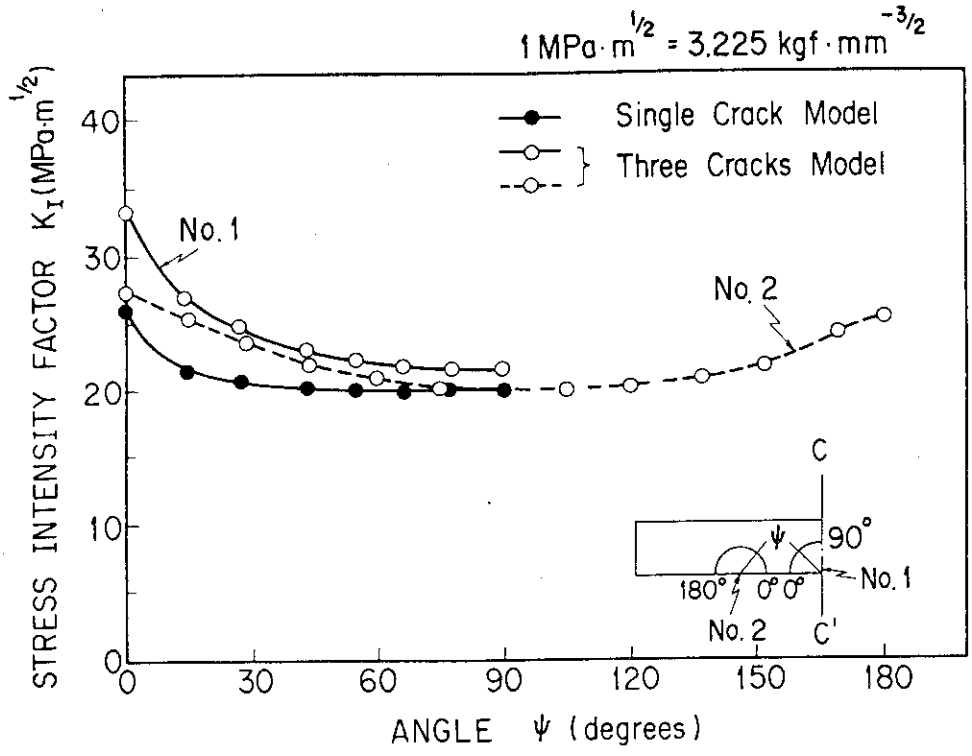

Fig. 4.22 Distribution of Stress Intensity Factors for Three Semi-Circular Cracks in a Plate Subjected to Tensile and Bending Forces

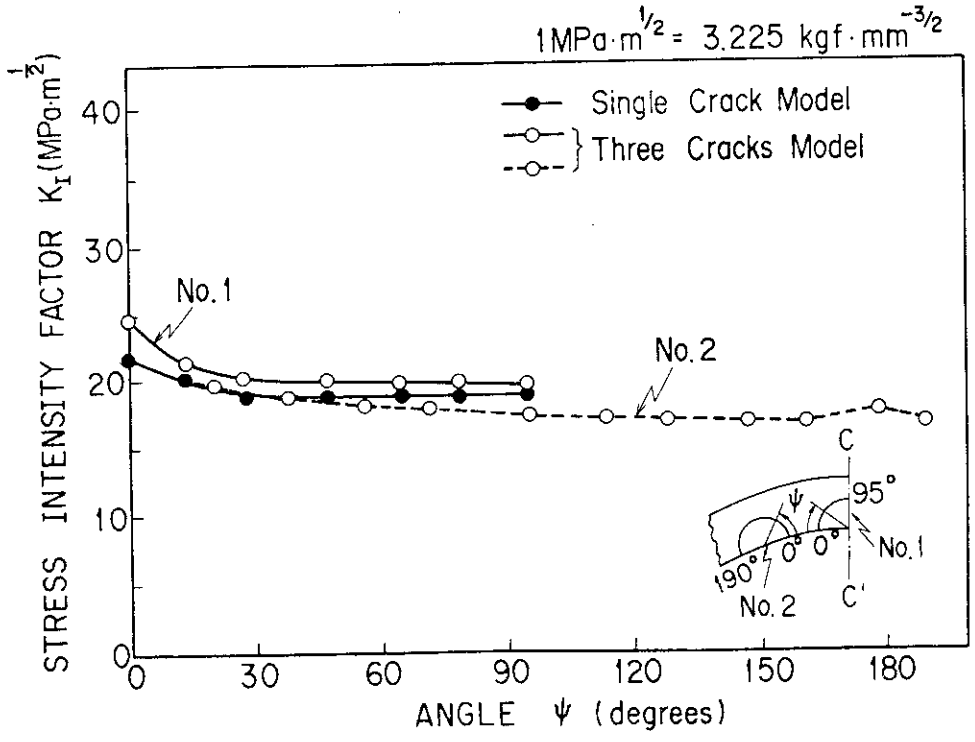

Fig. 4.23 Distribution of Stress Intensity Factors for Three Circle-Shaped Cracks in Inner Surface of a Cylinder Subjected to Shear Force

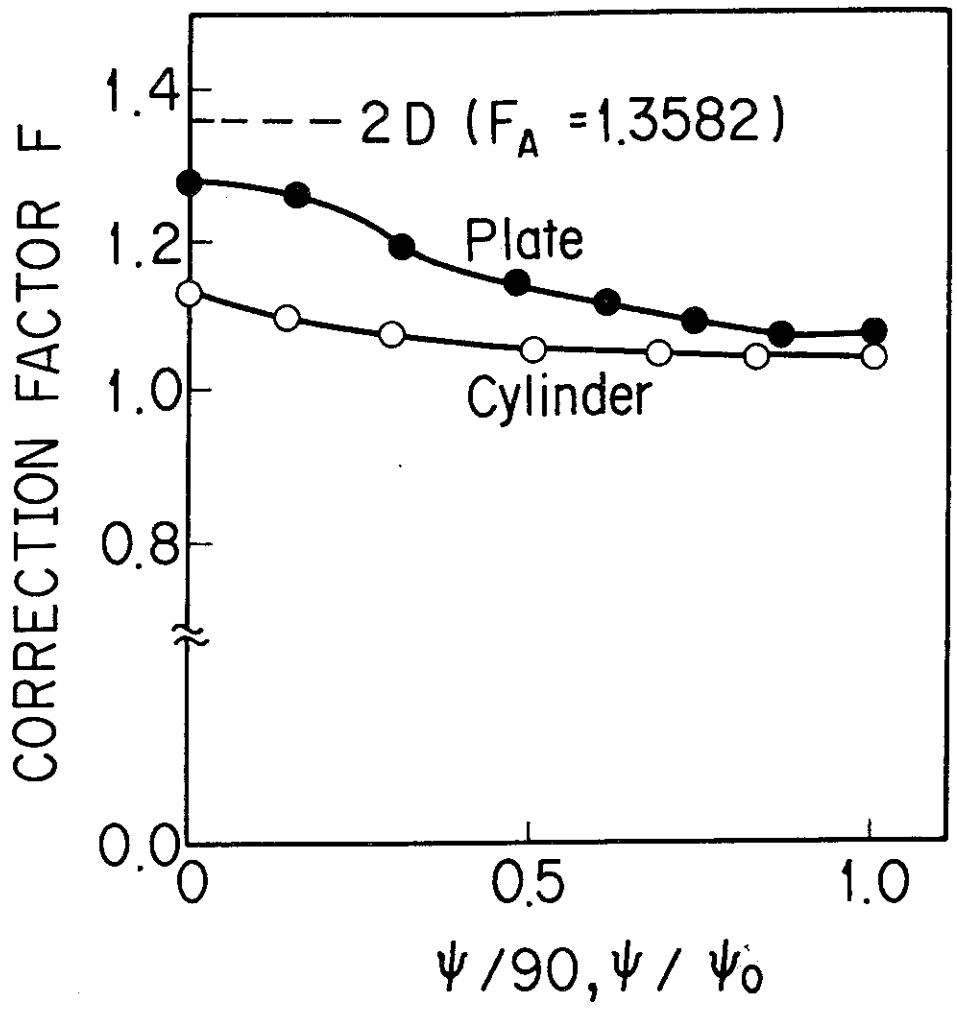

Fig. 4.24 Comparison of the Present Results with 2-Dimensional Solution

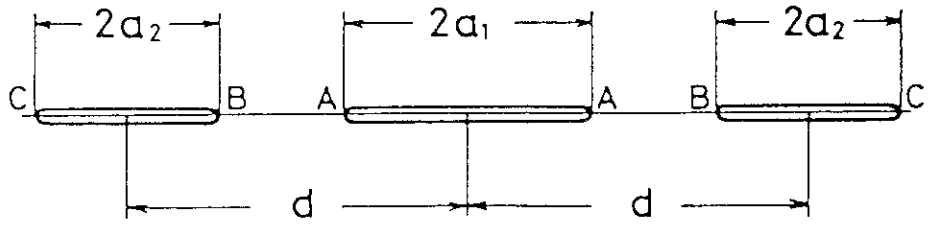

Fig. 4.25 Three Symmetric Cracks

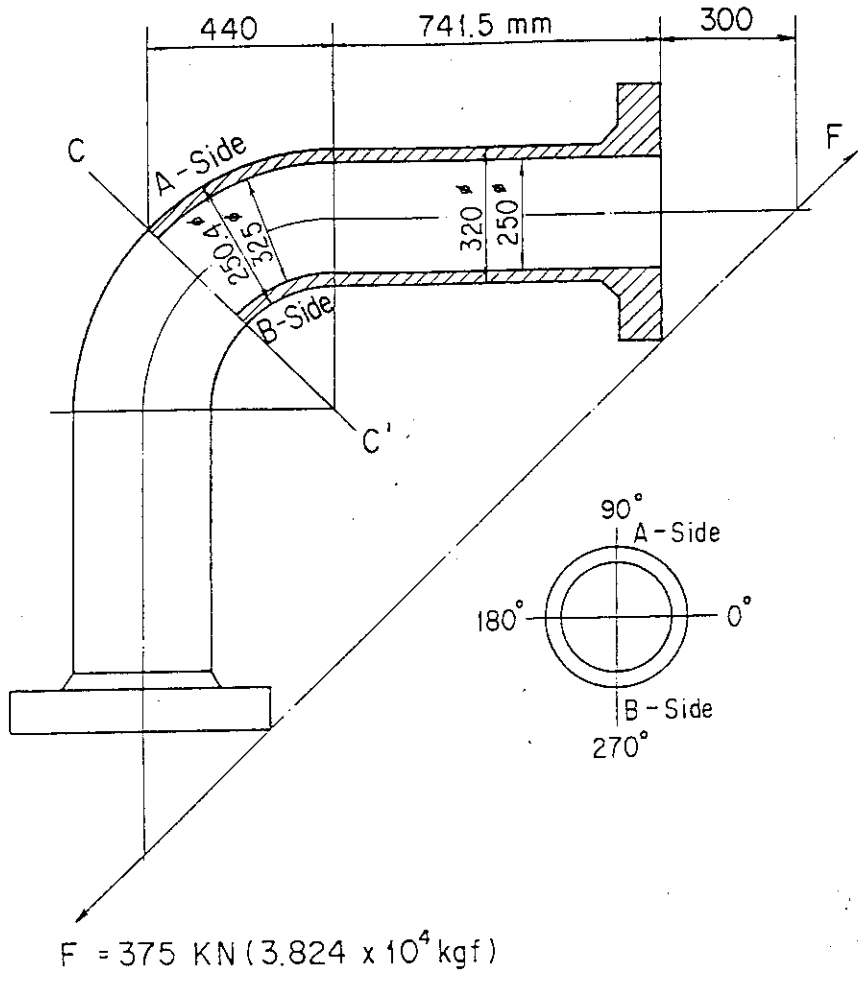

Fig. 4.26 Bend Pipe with Two Ellipse-Shaped Cracks

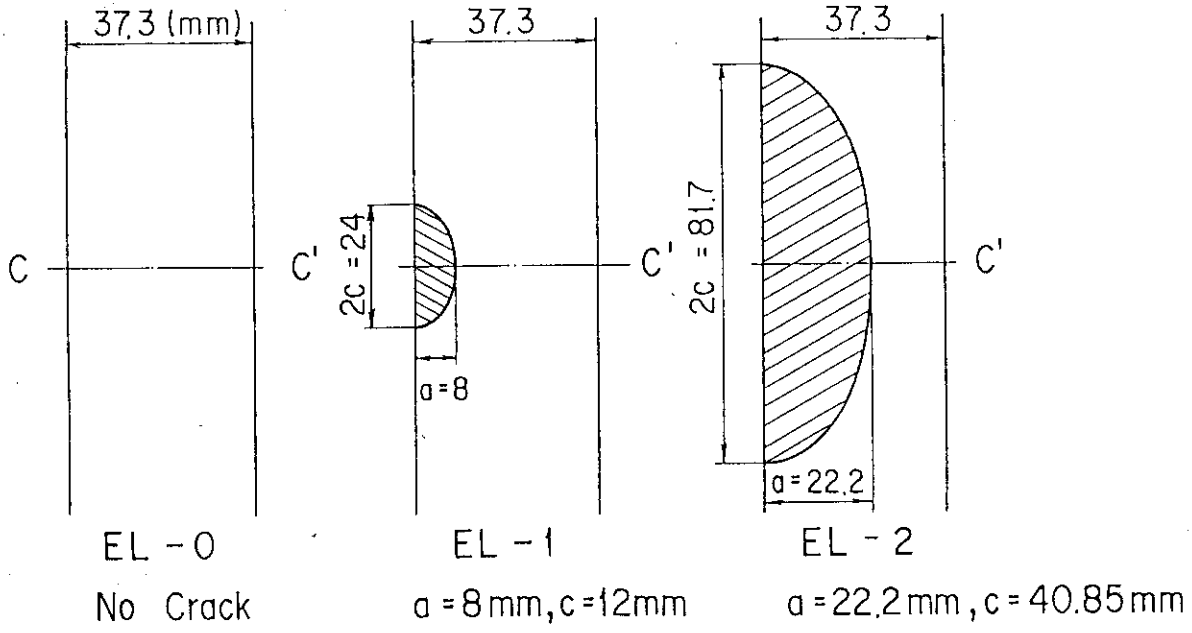

Fig. 4.27 Geometries of Cracks

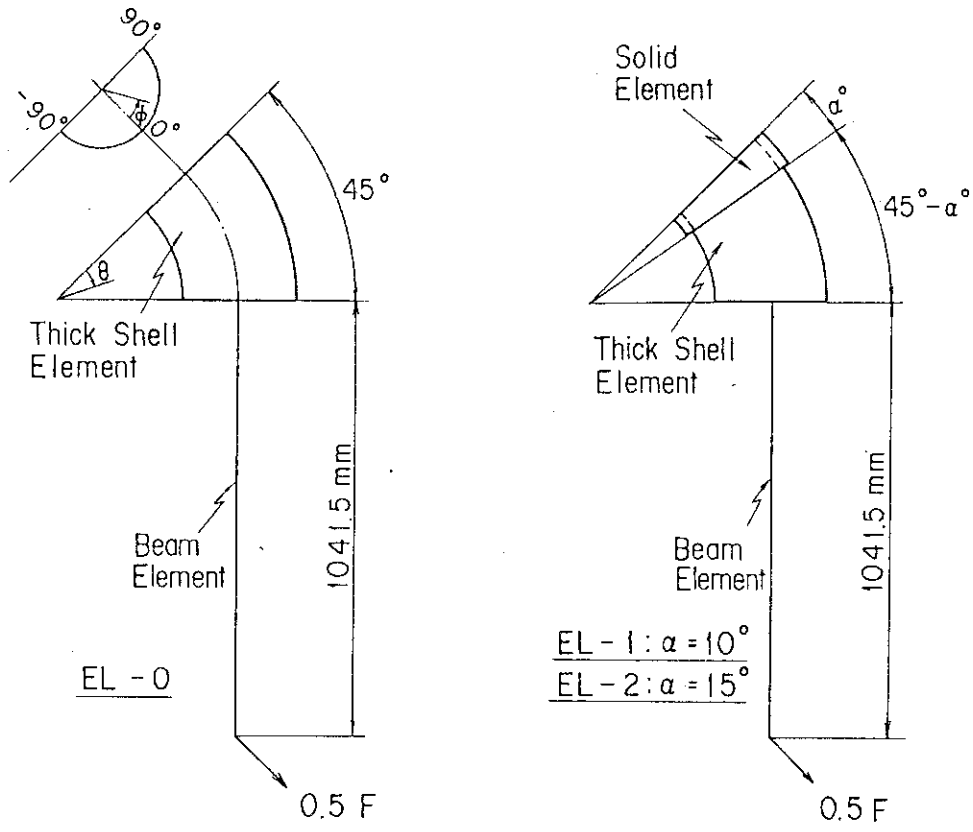

Fig. 4.28 Analytical Models for a Bend Pipe with Two Ellipse-Shaped Cracks

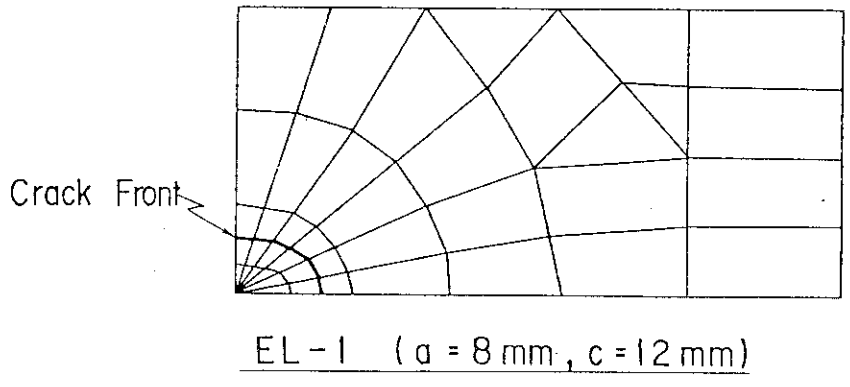

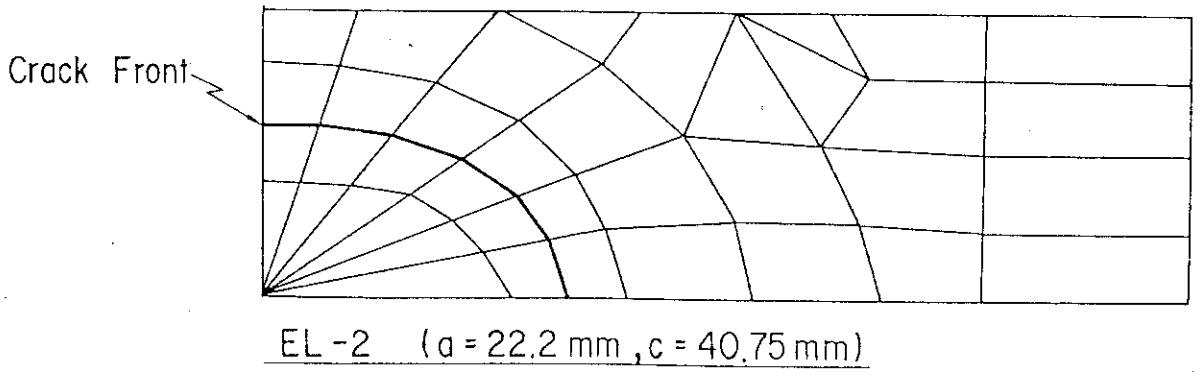

Fig. 4.30 Finite Element Meshes in the Surfaces with Crack

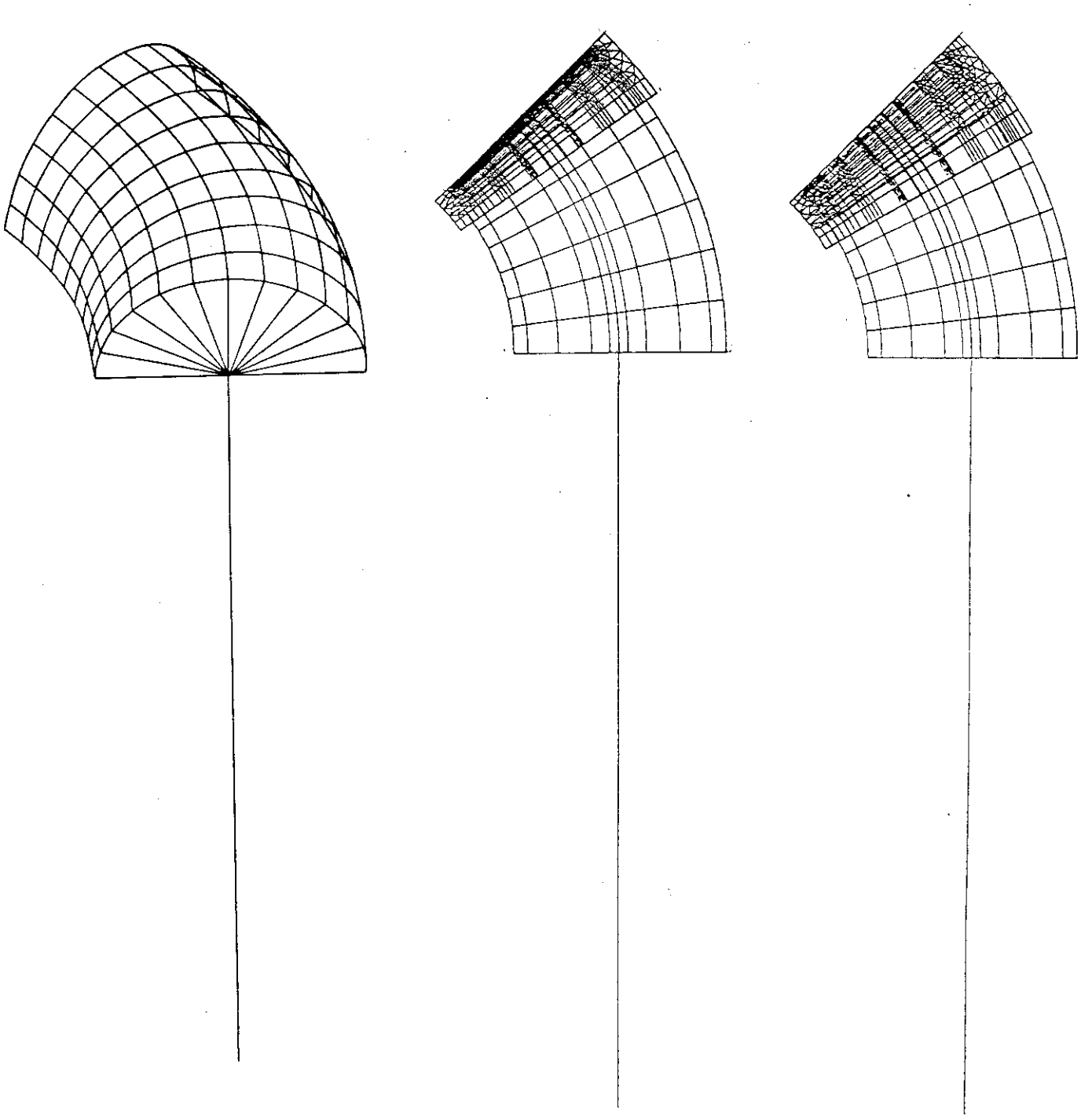

(a) EL-0 (b) EL-1 (c) EL-2

Fig. 4.29 Finite Element Meshes of a Bend Pipe

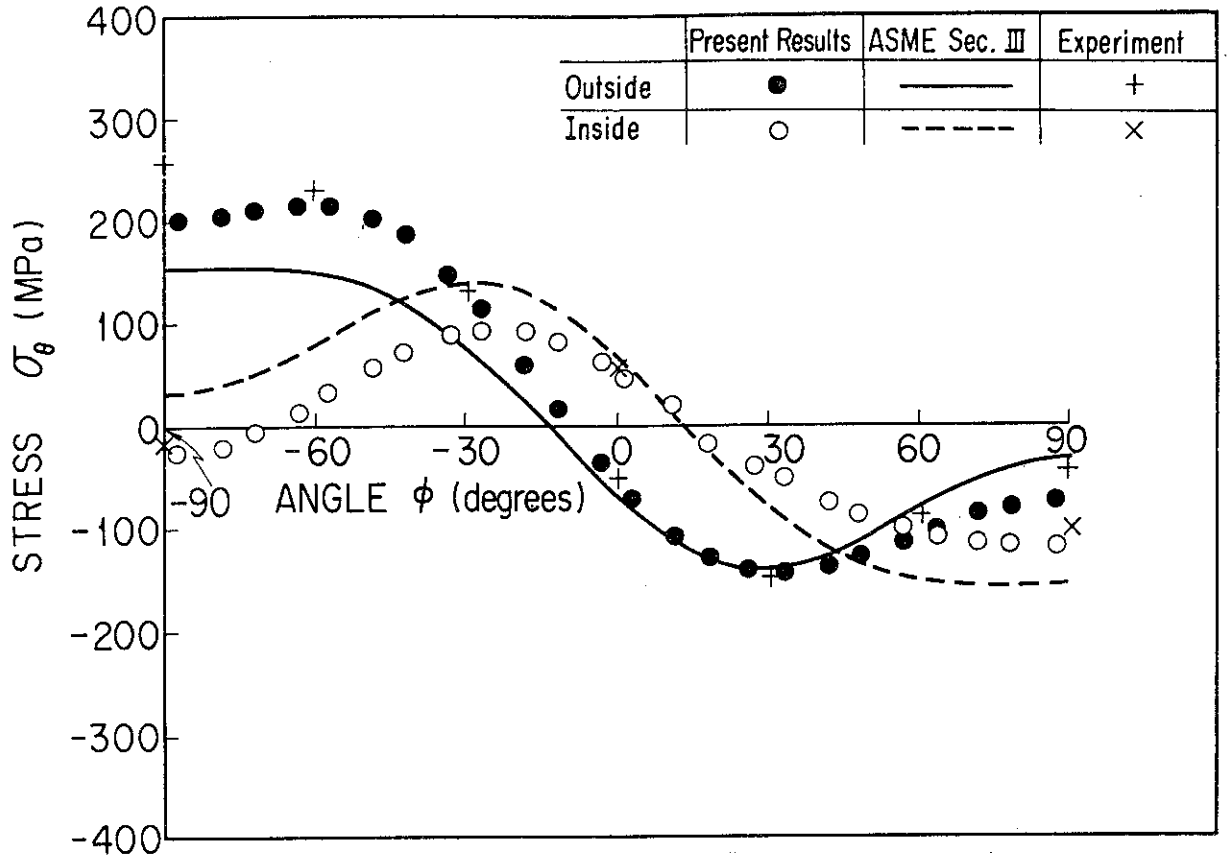

Fig. 4.31 Stress Distribution in an Elbow ---- σ_θ

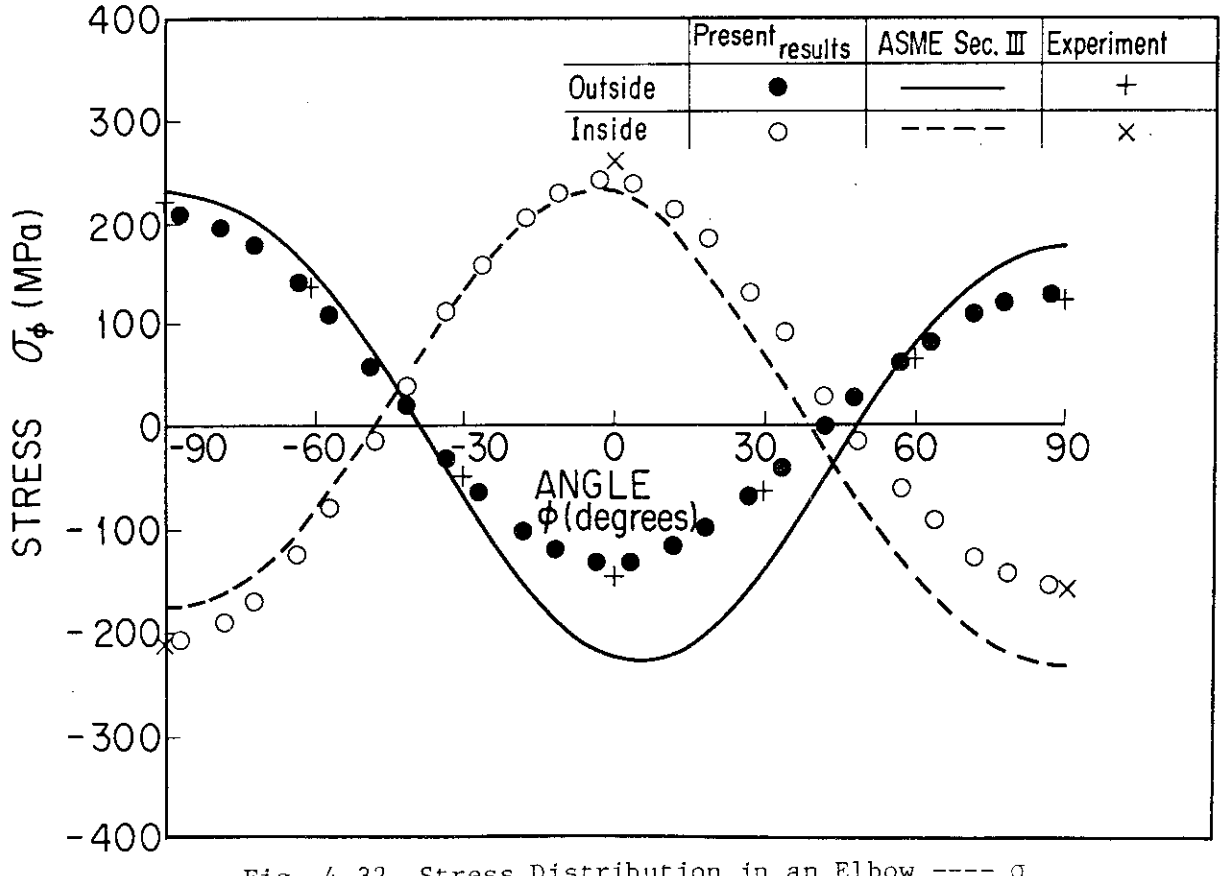

Fig. 4.32 Stress Distribution in an Elbow ---- σ_ϕ

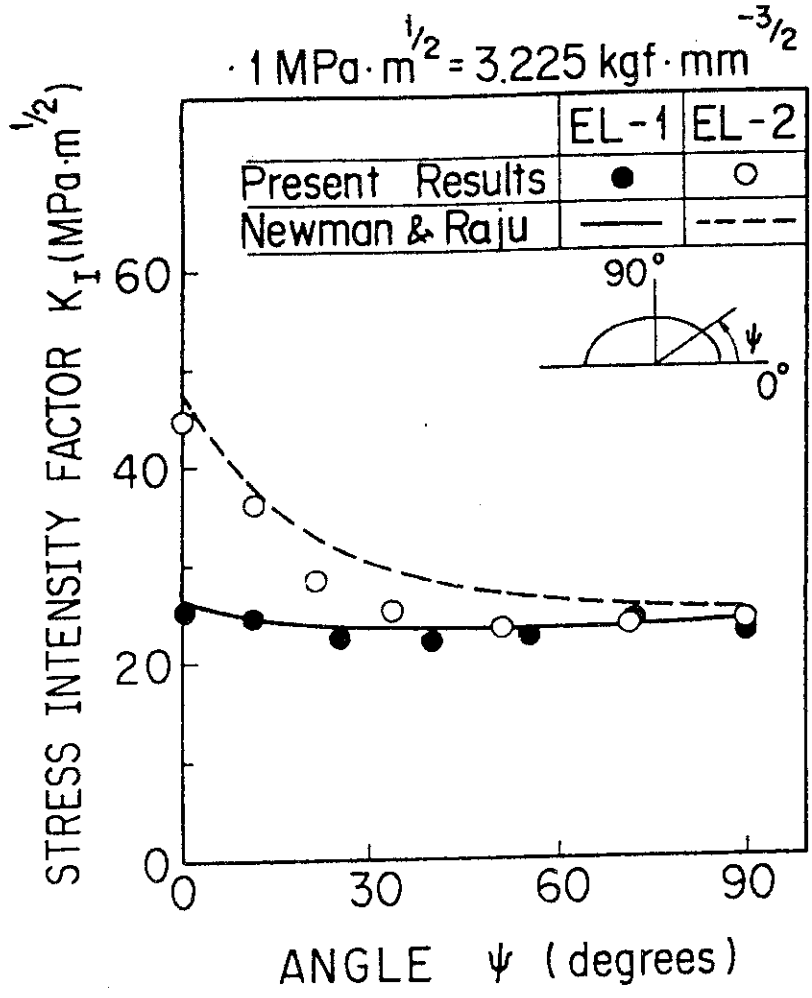

Fig. 4.33 Distribution of Stress Intensity Factors for Two Ellipse-Shaped Cracks in Inner Surface of an Elbow

5. Concluding Remarks

The stress intensity factors of surface cracks in various three-dimensional structures were calculated by the finite element program EPAS-J1 and were compared with other finite element solutions and those by the simplified estimation methods. The following conclusions were obtained from the analyses.

(1) Compared with the exact solution and other finite element solutions, the present results obtained by EPAS-J1 provide accurate stress intensity factors for an embedded circular crack and a semi-circular crack in a plate.

(2) For a semi-elliptical surface crack in inner surface of a pressurized cylinder, the present result obtained by EPAS-J1 agrees well with Atluri and Kathiresan's solution near the surface of a cylinder, and with Nishioka and Atluri's solution in the remainder of the region. On the other hand, the simplified estimation method using Newman and Raju's equations provides larger stress intensity factor than any other solutions compared with it except near the outer surface of the cylinder.

(3) For an ellipse-shaped crack in inner surface of a cylinder subjected to shear force, a larger difference can be found in the stress intensity factors at the surface point between the finite element method and the simplified estimation method, especially in the case of deep and large crack.

(4) The multiple cracks in a plate shows the larger interacting effect than those in a cylinder.

(5) For an ellipse-shaped cracks in inner surface of an elbow subjected to in-plane bending, the simplified estimation method using Newman and Raju's equations provides larger stress intensity factor for a large size crack than the present method by EPAS-J1. On the other hand, fairly good agreement is found between both results for a small size crack.

ACKNOWLEDGEMENT

The authors wish to acknowledge to Dr. S. Miyazono at the Japan Atomic Energy Research Institute for his useful comments.

5. Concluding Remarks

The stress intensity factors of surface cracks in various three-dimensional structures were calculated by the finite element program EPAS-J1 and were compared with other finite element solutions and those by the simplified estimation methods. The following conclusions were obtained from the analyses.

(1) Compared with the exact solution and other finite element solutions, the present results obtained by EPAS-J1 provide accurate stress intensity factors for an embedded circular crack and a semi-circular crack in a plate.

(2) For a semi-elliptical surface crack in inner surface of a pressurized cylinder, the present result obtained by EPAS-J1 agrees well with Atluri and Kathiresan's solution near the surface of a cylinder, and with Nishioka and Atluri's solution in the remainder of the region. On the other hand, the simplified estimation method using Newman and Raju's equations provides larger stress intensity factor than any other solutions compared with it except near the outer surface of the cylinder.

(3) For an ellipse-shaped crack in inner surface of a cylinder subjected to shear force, a larger difference can be found in the stress intensity factors at the surface point between the finite element method and the simplified estimation method, especially in the case of deep and large crack.

(4) The multiple cracks in a plate shows the larger interacting effect than those in a cylinder.

(5) For an ellipse-shaped cracks in inner surface of an elbow subjected to in-plane bending, the simplified estimation method using Newman and Raju's equations provides larger stress intensity factor for a large size crack than the present method by EPAS-J1. On the other hand, fairly good agreement is found between both results for a small size crack.

ACKNOWLEDGEMENT

The authors wish to acknowledge to Dr. S. Miyazono at the Japan Atomic Energy Research Institute for his useful comments.

REFERENCES

(1) Tada, H., Paris, P.C. and Irwin, G.R., The Stress Analysis of cracks Handbook, Del Research Corporation (1973)

(2) James, L.A., Estimation of Crack Extension in a Piping Elbow Using Fracture Mechanics Technique, J. Pressure Vessel Technology, Trans. ASME Ser. J., Vol. 96, No. 4 (1974), pp. 273-278.

(3) Miyazaki, N., Watanabe, T and Yagawa, G., Efficient Computer Program EPAS-J1 for Calculating Stress Intensity Factors of Three-Dimensional Surface Cracks, JAERI 1276 (1982)

(4) Henshell, R. D. and Shaw, K. G., Crack Tip Finite Elements Are Unneccessary, Int. J. Num. Meth. Eng. Vol. 9 (1975), pp. 495-507

(5) Hellen, T.K., On the Method of Virtual Crack Extensions, Int. J. Num. Meth. Eng., (1975), pp. 187-207.

(6) Irwin, G.R., Crack-Extension Force for a Part-Through Crack in a Plate, J. Appl. Mech., Trans. ASME Ser. D, Vol. 29, No. 4 (1952), pp. 651-654,

(7) Smith, F.W. and Alavi, M.J., Stress Intensity Factors for a Penny Shaped Crack in a Helf Space, Eng. Fract. Mech, Vol. 3, No. 3 (1971), pp. 241-254.

(8) Smith, F.W., Emery, A.F. and Kobayashi, A.S., Stress Intensity Factors for Semi-Ciraular Cracks, Part 2 — Semi-Infinite Solid, J. Appl. Mech., Trans ASME Ser. E, Vol. 34 (1967), pp. 953-959

(9) Kobayashi, A.S., Crack-Opening Displacement a Surface Flawed Plate Subjected to Tension or Plate Bending, Proc. Second Int. Conf. on Mech Mat., ASM (1976), pp. 1073-1077.

(10) Tracey, D.M., Finite Element for Three-Dimensional Elastic Crack Analysis, Nucl. Eng. and Des., Vol. 26 (1974), pp. 282-290.

(11) Newman, J.C. and Raju, I.S., Analyses of Surface Cracks in Finite Plate under Tension or Bending Loads, NASA-TP-1578 (1979).

(12) Heliot, J. and Labbens, R.C., Results for Benchmark Problem 1, The Surface Flaw, Int. J. Fract. 15 (1979), pp. R197-R202.

(13) Smith, F.W., Stress Intensity Factors for a Semi-Elliptical Surface Flaw, Boeing Airplane Co., Structural Development Research Memorandum No. 17 (1966).

(14) Sakakibara, Y., Imazu, A., Nagata, T. and Okabayashi, K., Fatigue Crack Program from Surface Flaw of Elbows, Trans. 6th Int. Conf. on Struct. Mech. in Reactor Technology (1981), E7/3

(15) Soya, I., Kashimura, H., Hagiwara, Y., Sato, M and Minami, K., On the Brittle Fracture Initiation from a Surface Crack at Welded Joint., J. Soc. Navel Architects of Japan, 140 (1976), pp. 223-232.

(16) Shah, R.C. and Kobayashi, A.S., On the Surface Flaw Problem, "The Surface Crack: Physical Problems and Computational Solutions", Edited by J.L. Swedlow, ASME (1972), pp. 79-124.

(17) Kawahara, M., Kurihara, M. and Arakida, F., Safety Assessment of Fatigue Failure in Structural Members Containing Flaws, Nippon Kokan Technical Report No. 78, (1978), pp. 67-79.

(18) Scott, P.M. and Thorpe, T.W., A Critical Review of Crack Tip Stress Intensity Factors for Semi-Elliptic Cracks, Fatigue of Eng. Mat. and Struct., Vol. 4 (1981), pp. 291-309.

(19) Raju, I.S. and Newman, J.C., Stress Intensity Factors for a Wide Range of Semi-Elliptical Surface Cracks in Finite Thickness Plates, Eng. Fract. Mech., Vol. 11 (1979), pp. 817-829.

(20) Koterazawa, R. and Minamikawa, S., Stress Intensity Factors of Semi-Elliptical Surface Cracks in Bending, J. Soc. Mat. Sci. Japan, Vol. 26 (1977), pp. 1-7.

(21) Ando, Y., Yagawa, G. and Ishihara, K., Three-Dimensional Fracture Analysis of Pressure Vessel Steel Plate Subjected to Thermal Shock, to appear in Trans. JSME.

(22) Yagawa, G. and Nishioka, T., Superpostion Method for Semi-Circular Surface Crack, Int. J. Solids Struct. Vol. 16 (1980), pp. 585-595

(23) Yagawa, G., Ichimiya, M. and Ando, Y., Two and Three-Dimensional Analysis of Stress Intensity Factors Based on Discretization Error in Finite Elements, Proc. 1st Conf. on Num. Meth. in Fract. Mech. (1978), pp. 249-269.

(24) Atluri, S.N. and Kathiresan, K., 3D Analysis of Surface Flaws in Thick-Walled Reactor Pressure Vessels Using Displacement-Hybrid Finite Element Method, Nucl. Eng. and Des. (1979), pp. 163-176

(25) Blackburn, W.S. and Hellen, T.K., Calculation of Stress Intensity Factors for Elliptical and Semi-Elliptical Cracks in Block and Cylinder, CEGB Report No. RD/B/N3103 (1974)

(26) Kobayashi, A.S., Polvnicha, N., Emery, A.F. and Love, W.J., Inner and Outer Crack in Internally Pressurized Cylinders, J. Pressure Vessel Technology, Trans. ASME Ser. J, Vol. 99 (1977), pp. 83-89

(27) Nishioka, T. and Atluri, S. N., Analysis of Surface Flaw in Pressure Vessels by a New 3-Dimensional Alternating Method, "Aspects of

Fracture Mechanics in Pressure Vessels and Piping", Edited by Palusamy, S.S. and Sampath, S.G., ASME PVP-Vol. 58 (1982), pp. 37-48.

(28) Murakami, Y. and Nishitani, H., Stress Intensity Factors for Interacting Two Equal Semi-Elliptical Surface Cracks in Tension, Trans. JSME, Vol. 47, No. 415 (1981), pp. 295-303.

(29) Murakami, Y. and Nemt-Nasser, S., Interacting Dissimilar Semi-Elliptical Surface Flaw under Tension and Bending, Eng. Fract. Mech., Vol. 16, No. 3 (1982), pp. 373-386.

(30) Shibata, K., Oba, T., Kawamura, R., Yokoyama, N. and Miyazono, S., Fatigue Test Results of Bend Pipes (EL-4, EL-5) (1982) ---- Unpublished Report